RESEARCH MEMORANDUM

PERFORMANCE CHARACTERISTICS AT MACH NUMBERS TO 2.00 OF VARIOUS TYPES OF SIDE INLETS MOUNTED ON FUSELAGE OF PROPOSED SUPERSONIC AIRPLANE

III - NORMAL-WEDGE INLET WITH SEMICIRCULAR COWL

By Fred T. Esenwein

Lewis Flight Propulsion Laboratory
Cleveland, Ohio

NATIONAL ADVISORY COMMITTEE
FOR AERONAUTICS

WASHINGTON

October 16, 1952

NACA RM E52H20

NATIONAL ADVISORY COMMITTEE FOR AERONAUTICS

RESEARCH MEMORANDUM

PERFORMANCE CHARACTERISTICS AT MACH NUMBERS TO 2.00 OF VARIOUS TYPES OF SIDE INLETS MOUNTED ON FUSELAGE OF PROPOSED SUPERSONIC AIRPLANE

III - NORMAL-WEDGE INLET WITH SEMICIRCULAR COWL

By Fred T. Esenwein

SUMMARY

As part of a general investigation of side inlets for supersonic speeds, inlets utilizing two-dimensional compression wedges mounted normal to the fuselage surface were investigated with ram-type scoops for partial removal of the boundary layer. Two compression-wedge angles were included to simulate fixed positions of a variable-geometry configuration. The research was conducted in the NACA Lewis 8- by 6-foot supersonic tunnel at Mach numbers of 0, 0.63, and 1.50 to 2.00 for a range of angles of attack from -6° to 12° using a quarter-scale model of the forward part of the fuselage of a proposed supersonic airplane. The Reynolds numbers of the investigation were approximately 18×10^{6} and 29×10^{6} based on the length of fuselage ahead of the inlets for Mach numbers of 0.63 and 1.50 to 2.00, respectively.

Results of the investigation indicated pressure recoveries of approximately 0.92 and 0.84 for the design angle of attack at Mach numbers of 1.50 and 2.00, respectively. For comparable boundary-layer control, these performance characteristics represented a substantial increase when compared with ramp and half-conical, spike-type side inlets of the present series of investigations. At angles of attack, however, sensitivity to cross-flow effects due to the particular circumferential location of the inlets resulted in severe decreases in pressure recovery, especially at the higher free-stream Mach numbers.

At a Mach number of 0.63 inlet-pressure recoveries of the order of 0.96 were obtained for mass-flow ratios of approximately 1.0 with negligible angle-of-attack effects indicated at the maximum angle of 6°. For take-off operation, however, large losses in performance with increasing inlet flow resulted in very low pressure recoveries; and to avoid excessive losses in engine performance, some type of auxiliary inlet would probably be required.

INTRODUCTION

The large losses in inlet total-pressure recovery, which were associated with incomplete removal of the boundary layer ahead of the half-conical spike inlets of references 1 and 2, were also observed for the ramp-type inlets of reference 3. For both types of inlets pressure recoveries of the order of those attainable with well designed nose inlets could be realized only with complete removal of the boundary layer. The design of boundary-layer-removal systems to provide adequate control for the wide range of possible inlet locations, fuselage shapes, and conditions of operation may well be impractical and side inlets less sensitive to boundary-layer effects would be desirable.

Techniques studied for improving the performance of side inlets with incomplete boundary-layer removal included elimination of large turning of the low-energy air entering the diffuser and utilization of the pressure gradient produced with supersonic compression to force the boundary layer around the inlet. In addition to these possible methods for minimizing boundary-layer effects, the desire to obtain the supersonic compression along surfaces relatively free of boundary layer led to the design of inlets employing two-dimensional compression wedges mounted normal to the fuselage surface.

Results obtained from the experimental investigation of several normal wedge-type inlets mounted on the triangular-shaped fuselage of reference 3 are presented herein. The investigation was conducted in the NACA Lewis 8- by 6-foot supersonic tunnel for a range of mass flows and angles of attack from -6° to 12° at free-stream Mach numbers of 0, 0.63, and 1.50 to 2.00.

SYMBOLS

The following symbols are used in this report:

A area

C_D model-drag coefficient based on maximum fuselage cross-sectional area of 1.784 sq ft. (Model drag is defined as the measured balance force minus the internal thrust and the base force where the internal thrust is change in total momentum from free stream to diffuser discharge of air passing through inlets.)

h height of boundary-layer scoop

M Mach number

m mass flow

[redacted]

P	total pressure (corrected for losses across shock where necessary)
P'	pitot pressure
p	static pressure
V	velocity
y	height normal to surface in plane of survey
α	fuselage angle of attack
β	local angle of flow measured with respect to inlet center line
δ	boundary-layer thickness defined to extend to 0.99 of the undisturbed velocity adjacent to the boundary layer
ρ	density

Subscripts:

B	boundary-layer bleed duct
c	canopy
i	inlet station corresponding to minimum flow area
max	maximum
p	projected frontal area
0	free stream
1	inlet rake survey, x = 5.94 in.
2	diffuser-discharge rake survey, model station 97.25

Pertinent mass-flow ratios:

$\frac{m_2}{m_0} = \frac{m_2}{\rho_0 V_0 A_p}$ ratio of mass flow passing through inlet to mass flow passing through free-stream tube of cross-sectional area equal to projected inlet frontal area of 0.0884 sq ft. (Similar mass-flow ratios determined for boundary-layer bleed scoops are based on projected frontal area of bleed scoops of 0.0246 sq ft.)

[redacted]

$\frac{m_2}{m_c} = \frac{m_2}{\rho_c V_c A_p}$ ratio of mass flow passing through inlet to mass flow (at local canopy conditions) passing through stream tube of cross-sectional area equal to projected inlet frontal area of 0.0884 sq ft. (Similar mass-flow ratios determined for boundary-layer bleed scoops are based on projected frontal area of bleed scoops of 0.0246 sq ft.)

$\frac{m_2}{m_i} = \frac{m_2}{\rho_0 V_0 A_i}$ ratio of mass flow passing through inlet to mass flow passing through free-stream tube of cross-sectional area equal to inlet minimum flow area of 0.0784 sq ft for 8°-wedge inlet

$\frac{m_2}{m_{2,max}}$ ratio of mass flow passing through inlet to mass flow measured at critical inlet flow

APPARATUS AND PROCEDURE

The quarter-scale model of the fuselage of the supersonic airplane reported in reference 3 was used for this investigation. A sketch of the model showing typical body cross sections and principal dimensions is presented in figure 1. A cross-sectional view of one of the main air ducts and the corresponding boundary-layer bleed duct is presented in figure 2(a). Ram-type boundary-layer scoops (h = 0.44 in.) were employed with internal ducts designed primarily to handle engine cooling-air flow. A more complete discussion of the model characteristics is included in reference 3.

Details of the normal-wedge inlets are shown in figure 2(b). The 14°- and 8°-half-angle compression wedges were selected to simulate fixed positions of a possible variable-geometry design for free-stream Mach numbers of 2.00 and 1.50, respectively. The internal inlet contours were designed to be parallel to the surfaces of the 14°-half-angle wedge as far back as the maximum cross section of the wedge and relatively sharp inlet leading edges were used to avoid internal contraction. As discussed in reference 3, the inlets were canted downward at 2° with respect to the fuselage to provide approximate alinement with the local flow near the cruise angle of attack (α = 3°).

The geometrical area variation of the main ducts from the plane of the inlet to the station corresponding to the engine face is presented in figure 3 for both the 14°- and 8°-wedge inlets. Typical duct cross sections are included for the 14°-wedge configuration showing the gradual transition from the divided semicircular section at the inlet to the circular cross section at the duct discharge.

[redacted]

Details of the several boundary-layer-removal systems included in the investigation can be seen in the photographs of figure 4. Ram-type scoops with sides (fig. 4(a)), sides removed (fig. 4(b)), and with the plates between the bleed and main ducts (herein referred to as "splitter plates") swept (fig. 4(c)) were investigated with the 14°-wedge design. Additional tests were conducted with the boundary-layer scoop faired ahead of the inlets to permit operation with no boundary-layer removal (fig. 4(d)). For the 8°-wedge design only the ram scoops with sides and with the swept splitter plates were investigated.

The mass flows through the inlets and the boundary-layer scoops were varied by means of remotely controlled plugs attached to the model sting. Model forces, which did not include the forces on the plugs, were measured with a three-component strain gage balance located inside the model.

Total pressure measurements were made at the inlet station (figs. 2(a) and 4(a)) of one inlet by means of 20 tubes and at the station corresponding to the face of the engine for each main duct with 33 pitot tubes. Additional total head rakes were used to determine the flow characteristics at the exit of each boundary-layer bleed duct. Average total pressures were obtained from an area weighting and were used to calculate the mass flows through the inlets and boundary-layer scoops based on the areas at the choked exits. Diffuser-discharge Mach numbers were evaluated using one-dimensional area ratios between the sonic discharge and the rake station. Model base pressures were measured by means of 13 static orifices, and the base force was calculated using an arithmetic average of these pressures, which were found to remain essentially constant across the base of the model for all conditions of operation.

The investigation at a Mach number of 0.63 was conducted by operating the tunnel subsonically. For take-off (zero forward speeds), a range of inlet air flows was obtained by attaching the model discharge ducts to the tunnel exhauster equipment as discussed in reference 3.

The Reynolds numbers of the investigation were approximately 18×10^6 and 29×10^6 based on the length of fuselage ahead of the inlets for Mach numbers of 0.63 and 1.50 to 2.00, respectively.

RESULTS AND DISCUSSION

Supersonic Performance Characteristics

Cruise angle of attack ($\alpha = 3^\circ$). - Pitot and total pressure ratio contours obtained from a survey of the flow upstream of the inlets are shown in figure 5 for Mach numbers of 1.50 and 2.00. The total-pressure

ratio P_c/P_0 was calculated assuming the static pressure at the base of the rake to be constant in the plane of survey. Indicated total-pressure ratios slightly greater than 1.0 (fig. 5(b)) are probably associated with inaccuracies in the assumed static pressure outside the boundary layer. Within the accuracy of these data, the results of the survey indicate essentially free-stream total pressure ahead of the inlets except in the region influenced by the fuselage boundary layer.

The boundary-layer thickness δ, which is represented by the dashed line in figure 5, is shown to be approximately 0.8 inch in thickness and nearly uniform across the face of the inlet for both Mach numbers. Similar trends and approximately the same boundary-layer thickness were noted for Mach numbers of 1.70 and 1.90. For the boundary-layer-scoop height of 0.44 inch, therefore, the resultant h/δ was 0.55 at the cruise angle of attack.

Inlet mass-flow ratios, total-pressure recoveries, and model-drag coefficients obtained from the investigation of the 14°- and 8°-wedge inlets, utilizing the boundary-layer scoops with sides and the 14°-wedge inlet with the faired canopy and no boundary-layer control, are presented in figure 6. Mass-flow ratios m_2/m_c based on the results of the survey of the flow immediately ahead of the inlets, such that $m_2/m_c = 1.0$ represents the maximum mass flow that could be captured by the inlets, are also included. The boundary-layer bleed flows for partial boundary-layer control were selected on the basis of assumed cooling-air flow requirements.

The characteristics for the 14°-wedge inlet ($h/\delta = 0.55$), presented in figure 6(a), indicate a maximum pressure recovery of 0.85 for subcritical inlet operation at the design Mach number of 2.00. Near critical flow, however, recoveries of approximately 0.82 were obtained. These pressure recoveries are only slightly below the results reported in references 3 and 4 for the ramp and half-conical spike-type side inlets with complete boundary-layer removal. The somewhat lower pressure recoveries obtained with the normal-wedge inlet were determined to result solely from the low energy of the boundary-layer air entering the inlet.

A maximum mass-flow ratio $(m_2/m_c)_{max}$ of 0.84 for Mach number 2.00 resulted from designing the inlet with the oblique shock ahead of the cowl lip and represents 16 percent supersonic air spillage at critical flow. Reductions in the maximum mass flow with decreasing free-stream Mach number due to the increased spillage behind the oblique shock produced a slight increase in model drag for supercritical inlet flow. With subcritical inlet operation, the increase in model-drag coefficient can be attributed to the drag associated with the spillage of air behind the normal shock.

The pressure recoveries presented in figure 6(b) for the 8°-wedge inlet at a Mach number of 1.50 are approximately equal to the results obtained with the 14°-wedge inlet. At a Mach number of 2.00, however, pressure recoveries of the order of 3 to 4 percent lower are observed over most of the subcritical range. The better performance of the 14°-wedge inlet at the higher Mach numbers might be expected, because of the more nearly optimum supersonic compression for the local conditions ahead of the inlet.

In contrast to the relatively low maximum mass-flow ratio m_2/m_c of 0.72 for the 14°-wedge inlet at Mach number 1.50, decreasing the compression angle to 8° resulted in an increase in mass-flow ratio to 0.89 as shown in figure 6(b). This increase in mass-flow ratio occurred because of the reduced air spillage behind the oblique shock as the wedge angle was decreased. Similar increases in maximum mass-flow ratios were obtained at the higher Mach numbers. As a result of the reduced supersonic air spillage over the Mach number range, slightly lower minimum model drags were obtained for the 8°-wedge inlet as compared with the 14° configuration.

Results obtained from the investigation of the 14°-wedge inlet with the canopy faired to be tangent to the upper surface of the boundary-layer scoop ($h/\delta = 0$) are presented in figure 6(c). Although peak pressure recoveries of 0.80 and 0.92 were obtained at Mach numbers of 2.00 and 1.50, respectively, for low inlet flows, pressure recoveries of only 0.71 at a Mach number of 2.00 and 0.80 at a Mach number of 1.50 were obtained for critical flow. Compared with the results presented in figure 6(a) for the 14° inlet with partial boundary-layer removal, decreases in pressure recovery of the order of 10 percent result from the increased boundary layer entering the inlet. This loss in total-pressure recovery is only slightly greater than the estimated value of 8 percent which would result because of the low energy of the additional boundary layer captured by the inlet.

The maximum inlet mass flows m_2/m_c of approximately 0.83 at a Mach number of 2.00 and 0.74 at a Mach number of 1.50 are in agreement with the results obtained for the $h/\delta = 0.55$ configuration (fig. 6(a)). As indicated by the lower values of m_2/m_0, however, the actual mass flow through the inlets has been reduced at critical conditions because of the increased quantity of boundary-layer air passing through the inlets. Comparable minimum model drags for the two inlets reveals the higher pressure recoveries with boundary-layer control were attained with no increase in drag.

Stable inlet flow was obtained throughout the range of subcritical and supercritical operation for the three configurations. The large region of stable subcritical operation obtained with the 14°-wedge inlets

[redacted]

may be associated with the oblique shock which falls well ahead of the cowl lip (reference 5). For the 8°-wedge inlet, however, the oblique shock nearly intersects the cowl lip at a Mach number of 2.00 and the stable operation at subcritical inlet flows cannot be explained with the vortex-sheet criteria of reference 5.

The variation of inlet pressure recovery and model drag over a range of boundary-layer-bleed mass flows is summarized in figure 7 for the 14°- and 8°-wedge inlets having an h/δ of 0.55. Included on figure 7(a) for zero boundary-layer removal are data obtained with the boundary-layer scoops faired to provide an h/δ of zero. Lines of constant bleed mass-flow ratio $(m_2/m_c)_B$ based on the results of the flow survey ahead of the boundary-layer scoops have been included.

For the 14°-wedge inlet (fig. 7(a)), increases in pressure recovery from 0.79 to 0.84 were measured at a Mach number of 2.00 as the bleed mass-flow ratio $(m_2/m_c)_B$ was increased from approximately 0.10 to 0.70 while a negligible effect on drag was observed. Further increases in bleed mass flow resulted in a slight decrease in pressure recovery, although stable inlet flow was maintained. As indicated by the tailed symbols, near peak pressure recovery was realized for the rated-bleed-flow conditions previously presented in figure 6(a). For Mach numbers of 1.50 and 1.70 the greater degree of subcritical inlet flow indicated by the lower diffuser-discharge Mach numbers, shows a decreased effect of bleed-flow variations on the inlet pressure recovery. This trend has been determined to result primarily from the reduced triggering action of the boundary layer in the subsonic diffuser (reference 1) at the low internal velocities associated with the reduced inlet mass flows. It should be noted that while variations in model drags are significant at each free-stream Mach number, the relative magnitudes of the drag values should not be compared for the several Mach numbers inasmuch as they are a function of the diffuser-discharge Mach numbers selected. The data which were obtained with the faired canopy ($h/\delta = 0$) indicate no appreciable change in drag but somewhat larger losses in inlet recovery than would be obtained from an extrapolation of the results for the h/δ of 0.55 configuration.

Increases in inlet pressure recovery were also obtained for the 8°-wedge inlet with increasing bleed mass flows (fig. 7(b)). The somewhat greater sensitivity of pressure recovery to boundary-layer effects at the lower Mach numbers as compared with the 14°-wedge inlet is associated with the increased effect of boundary layer on the subsonic diffuser at the higher inlet mass flows (indicated by the higher value of M_2) at which these effects were determined.

The variation of inlet pressure recoveries corresponding to maximum thrust minus drag for a range of bleed-scoop-height to boundary-layer-thickness ratios h/δ is compared in figure 8 with the results obtained for the ramp-type inlets of reference 3. Evaluation of the maximum thrust-minus-drag conditions was made using the method discussed in reference 6. With comparable boundary-layer control the 14°-normal-wedge inlet resulted in higher pressure recoveries for the range of Mach numbers, as indicated in figure 8(a). For example, at a Mach number of 2.00 and an $h/\delta = 0.55$, a pressure recovery of 0.83 was obtained for the normal-wedge inlet as compared with a pressure recovery of 0.73 for the ramp-type inlet. Although not strictly comparable, the data obtained with the 13°-ramp inlet (ramp curved to 0° at inlet cowl) of reference 3, which have been included for the $h/\delta = 0$ condition, indicate similar results. As shown in figure 8(b), corresponding trends were observed for the 8° and 6° configurations at a Mach number of 1.50. The magnitudes of the differences in pressure recovery, however, were considerably smaller.

Some insight into the differences in performance for these two types of inlets can be obtained from the breakdown of total pressure losses into inlet $(\Delta P_{0,1}/P_0)$ and subsonic diffuser losses $(\Delta P_{1,2}/P_0)$, as shown in figure 9. With boundary-layer control $(h/\delta = 0.55)$, the inlet losses for the 14°-normal-wedge and ramp-type inlets were approximately equal (fig. 9(a)) and the higher pressure recoveries of the normal-wedge inlet were associated with the improved performance of the subsonic diffuser. The more nearly equal performance noted for the 8°-normal-wedge and 6°-ramp inlets (fig. 8(b)) resulted from the similar performance shown in figure 9(b) for both the inlets and the subsonic diffusers. With no boundary-layer control $(h/\delta = 0)$, the higher inlet pressure recoveries noted in figure 8(a) for the 14°-normal-wedge inlet as compared with the 13°-ramp configuration with the ramp faired to 0° at the inlet cowl, resulted from the lower inlet losses shown in figure 9(c), while the subsonic diffuser losses were comparable.

Analysis of these results indicates the lower inlet pressure recoveries of the 14°-ramp inlets result from the losses associated with the location of the large curvatures along the surface washed by the boundary layer, a characteristic of the ramp-type side inlets with large compression angles. Improvements in performance obtained with the normal-wedge inlets indicate the possibility of designing side inlets less sensitive to boundary-layer effects by avoiding large curvatures of the surface adjacent to the low-energy boundary-layer air entering the inlet.

Some details of the performance of the normal-wedge inlets are illustrated by the typical inlet total-pressure profiles presented in figure 10 for several conditions of operation. The low-energy air entering the inlets as a result of incomplete removal of the boundary layer can be noted along the splitter-plate surface. Although no large effects are observed due to the oblique-shock boundary-layer interaction

at the maximum inlet mass flows, some separation is seen to occur along the surface of the splitter plate in the vicinity of the compression wedge at the low mass flows (figs. 10(a) and 10(b)) when the normal shock interacts with the boundary layer. With no boundary-layer removal ($h/\delta = 0$), an increase in thickness of the boundary layer occurred with decreasing inlet mass flow; however, no flow separation was observed.

Contours of total-pressure ratio at the diffuser discharge (model station 97.25) for conditions corresponding to the inlet profiles are presented in figure 11. With supercritical inlet flow ($M_2 \geq 0.228$), total-pressure variations of the order of 13 percent were measured across the duct for the three inlet configurations. With slightly subcritical inlet flow ($M_2 < 0.228$), however, the total-pressure variations were reduced to less than 10 percent. The larger variations in total pressure across the duct with supercritical inlet flow are probably associated with separation effects resulting from the normal shock influence inside the diffuser.

The region of low-energy air which is located directly downstream of the splitter-plate surface can be attributed to the boundary-layer entering the inlet and to the relatively large curvature of the duct along this surface (see fig. 2). A core of high-energy air which results from the decreased boundary layer and lower curvature of the duct along the outer wall can be noted in quadrants 1 and 4 near the duct surface. Although no large wake effects were measured, slight irregularities in the contours are probably associated with flow disturbances due to the presence of the two-dimensional center body which divides the duct.

Additional inlet performance characteristics obtained with the modified boundary-layer bleed systems shown in figure 4 are compared in figure 12 with the results obtained when the ram-type scoops with sides were utilized. Successive increases in maximum inlet mass-flow ratios were observed at each Mach number as the sides of the bleed scoops were removed and the splitter plates were swept. Slight increases in inlet pressure recoveries were also obtained near critical mass flow for Mach numbers of 1.50 and 1.70 with some increase in drag. At a Mach number of 2.00, however, modifying the bleed system resulted in lower inlet recoveries for subcritical flow with no apparent effect on drag. These changes in inlet performance produced by removing the sides of the boundary-layer scoop are similar to the results noted in figure 7 when the bleed mass-flow ratio $(m_2/m_0)_B$ was increased to approximately unity. It appears, therefore, that the major contribution of the modified boundary-layer scoops is to permit the spillage of boundary-layer air along the sides of the scoops resulting in effective bleed-mass-flow ratios of approximately unity for the inlet while rated flow is maintained through the ducts.

Angle-of-attack characteristics. - Typical pitot-pressure contours measured ahead of the inlets are included in figure 13 for a range of

angles of attack from -6° to 12° at a Mach number of 2.00. Similar flow characteristics were noted at the lower supersonic Mach numbers. Values of local flow angles measured at station 67.5 in reference 3 are also tabulated in the following table to facilitate discussion of the angle-of-attack effects:

M_0	α	β
2.00	0°	-1°30'
	3°	1°30'
	6°	4°20'

Comparison of the results shown in figure 13 with the contours presented for the cruise angle of attack indicates small variations in boundary layer for angles of attack to 9°. At 12°, however, the boundary-layer thickness increased to approximately 1.5 inches and extended over nearly two-thirds of the inlet face; local values of h/δ as low as 0.30 resulted. As the model angle of attack was decreased to negative values, the boundary-layer thickness decreased, until at -6° local values of h/δ from 1.0 to 2.5 were attained across the face of the inlet.

The effect of positive angles of attack on inlet performance is indicated in figures 14(a) and 14(b) for the inlets which utilized boundary-layer scoops with sides. Comparable data are included in figure 14(c) for the 14° inlet with no boundary-layer removal. The slight increases in pressure recovery of approximately 1 to 3 percent which were obtained with the several inlets as the angle of attack was reduced from 3° to 0° appear to be associated with the decrease in boundary layer noted in figure 13 inasmuch as the local angle of cross flow at the inlet is of the same magnitude. The negligible decreases in pressure recovery obtained for angles of attack to 6° with nearly constant boundary layer ahead of the inlets, indicate that the inlet performance was not influenced adversely with angles of cross flow up to nearly 4.5°. For a 9° angle of attack, however, the decrease in pressure recovery with no apparent change in fuselage boundary layer can be attributed to the sensitivity of the inlet to cross-flow effects. Significant losses in inlet pressure recovery as the angle of attack was increased from 9° to 12° appear to be associated with the large changes in boundary layer shown in figure 13. Although the magnitudes of the local flow angles at the inlet were not determined for these high angles of attack, the cross flow also undoubtedly contributes to loss in performance.

Comparison of the inlet characteristics presented in figure 14(a) for the 14° wedge at a Mach number of 2.00 with the results presented in figure 14(b) for the 8° inlet at a Mach number of 1.50 indicates a smaller reduction in pressure recovery with angle of attack at the lower Mach

numbers. For example, losses in pressure recovery of approximately 12 percent are noted near critical flow at a Mach number of 1.50 as compared with 20 percent at a Mach number of 2.00 with increasing angles of attack from 3° to 12°. Comparable smaller changes in inlet mass-flow ratios were also noted for a Mach number of 1.50.

The results presented in figure 14(c) for the 14°-wedge inlet with no boundary-layer removal indicate losses in pressure recovery of approximately 12 percent near critical inlet flow as the angle of attack is increased from 3° to 12° at a Mach number of 2.00. Comparison of these results with the data presented in figure 14(a) for the inlet with boundary-layer control shows comparable inlet pressure recoveries at an angle of attack of 12°. Therefore, the improved performance noted with boundary-layer control at the cruise angle of attack appears to be offset by the greater sensitivity of the inlet to angle-of-attack effects, and equally low performance is obtained for both configurations at high angles of attack.

The influence of the angle of attack on the flow, in the vicinity of the inlet entrance, is summarized in figure 15. For zero angle of attack some separation is indicated adjacent to the splitter-plate surface for rake 2; while at the higher angles of attack, relatively small boundary layer is noted in this region and the region of separated flow has shifted to rake 3. Correlation of these results with the local inlet-flow angles tabulated previously and the pitot contour presented in figure 13, indicates the separation occurred along the leeward side of the wedge, downstream of the region of greatest fuselage boundary layer. In general, decreased separation effects were noted at a Mach number of 1.50 (fig. 15(b)). With no boundary-layer removal, the region of flow separation for the 14°-wedge inlet at a Mach number of 2.00 was observed to increase when compared with the results obtained with partial boundary-layer control.

At the diffuser discharge, the increase in the region of low-energy air, shown in figure 16 to occur downstream of the upper half of the inlet with increasing angles of attack, can be associated with the increased fuselage boundary layer (fig. 13). Similarly, the core of high-energy air which is observed to move to a position downstream of the lower half of the inlet can be explained from the influence of the shift in fuselage boundary layer and the variations in inlet-flow characteristics noted in figure 15. Comparable results were observed for the several inlet configurations over the range of angles of attack.

Limited performance characteristics obtained at negative angles of attack with the 14°-wedge inlet utilizing the swept splitter plate are presented in figure 17. The decrease in inlet pressure recovery over the range of air flows with negative angles of attack results from the flow separation along the leeward side of the wedge (fig. 18) which occurs

even though an effective h/δ of 1.0 was attained for an angle of attack of -6°. These decreases in inlet performance noted for both positive and negative angles of attack illustrate the relatively high sensitivity of the normal-wedge-type inlet to cross-flow effects. Relocation of the normal-wedge-type inlets in the plane of pitch would provide a means of avoiding cross flow and may eliminate the poor angle-of-attack characteristics.

Subsonic and Take-Off Performance Characteristics

Inlet pressure recovery and mass-flow characteristics at a Mach number of 0.63 are presented in figure 19 for angles of attack to 6°. Pressure recoveries from 0.99 to 0.95 were obtained throughout the range of inlet flows prior to choking at the minimum inlet area ($M_2 \approx 0.266$), and negligible angle-of-attack effects were observed. A pressure recovery of approximately 0.96 is indicated with inlet mass-flow ratios (based on inlet minimum area, A_i) of nearly 1.0. Results of an extrapolation of these data to the 5°-wedge angle, assumed to be the minimum attainable from practical considerations, have been included in figure 19. For these calculations, the pressure recoveries were assumed to be comparable for equivalent inlet mass-flow ratios and the resultant diffuser-discharge Mach numbers corresponding to the increased inlet minimum area were evaluated. The estimated performance for the 5°-wedge configuration indicated that the range of high inlet pressure recoveries can be extended significantly at subsonic speeds by means of the variable-geometry-type inlet.

Inlet characteristics at zero forward speeds (fig. 20) show large losses in inlet performance with increasing air flow, and, at take-off, pressure recoveries as low as 0.70 would result with the 8°-wedge inlet operating at mass-flow ratios $m_2/m_{i,max}$ of approximately 0.80. In this case, $m_{i,max}$ represents the maximum mass flow that could pass through the minimum inlet area if no losses occurred ahead of the inlet. The improvement in performance indicated by the data extrapolated to a 5°-wedge angle is small and large losses in thrust would result from use of this inlet with a turbojet engine at take-off unless auxiliary air intakes were available.

SUMMARY OF RESULTS

The performance characteristics of side inlets utilizing two-dimensional compression wedges normal to the fuselage surface and semicircular cowls were investigated in the 8- by 6-foot supersonic tunnel for a range of angles of attack from -6° to 12° at Mach numbers of 0, 0.63, and 1.50 to 2.00. Several ram-type scoops for partial removal of

the boundary layer ahead of the inlets were studied and the influence of the fuselage boundary layer on inlet performance was determined. The research which was conducted at a Reynolds number of approximately 29×10^6 for the supersonic Mach numbers (based on length of fuselage ahead of inlets) indicates:

1. Reduced sensitivity of side inlet performance to boundary-layer effects was obtained with the design of an inlet to provide supersonic compression in a plane normal to the surface washed by the fuselage boundary layer. The decreased turning of the low-energy boundary-layer air in the high Mach number regions of the inlet with this type of design (as compared with ramp and half-conical spike-type inlets) resulted in significant increases in pressure recovery.

2. Removing the sides of the ram-type boundary-layer scoops to provide bleed mass flows of unity and sweeping the leading edges of the splitter plates resulted in small increases in pressure recovery at Mach numbers of 1.50 and 1.70 with some increase in drag. At a Mach number of 2.00, however, decreases in pressure recovery were observed with negligible effect on drag.

3. Relatively large effects of cross flow for normal-wedge-type inlets were indicated by the decreases in pressure recovery of the order of 5 to 7 percent as the angle of attack was varied from 0° to -6° (decreasing fuselage boundary layer) at a Mach number of 2.00. These adverse effects resulted from flow separation along the leeward side of the wedge.

4. The decreases in pressure recovery with positive angles of attack to 9° were associated primarily with the cross-flow effects, whereas large losses at 12° probably resulted from the increased fuselage boundary layer.

5. Satisfactory inlet pressure recoveries of the order of 0.96 to 0.97 were indicated for a Mach number of 0.63 at mass-flow ratios of the order of unity, with negligible angle-of-attack effects to 6°.

6. For take-off operation very low inlet recoveries were obtained and large penalties in performance are indicated unless auxiliary air intakes are employed.

Lewis Flight Propulsion Laboratory
National Advisory Committee for Aeronautics
Cleveland, Ohio, July 18, 1952

[redacted]

REFERENCES

1. Goelzer, H. Fred, and Cortright, Edgar M., Jr.: Investigation at Mach number 1.88 of a Half of a Conical-Spike Diffuser Mounted as a Side Inlet with Boundary-Layer Control. NACA RM E51G06, 1951.

2. Wittliff, Charles E., and Byrne, Robert W.: Preliminary Investigation of a Supersonic Scoop Inlet Derived from a Conical-Spike Nose Inlet. NACA RM L51G11, 1951.

3. Valerino, Alfred S.: Performance Characteristics at Mach Numbers to 2.0 of Various Types of Side Inlets Mounted on Fuselage of Proposed Supersonic Airplane. I - Two-Dimensional Compression-Ramp Inlets with Semicircular Cowls. NACA RM E52E02, 1952.

4. Allen, J. L., and Simon, P. C.: Performance Characteristics at Mach Numbers to 2.0 of Various Types of Side Inlets Mounted on Fuselage of Proposed Supersonic Airplane. II - Inlets Utilizing Half of a Conical Spike. NACA RM E52G08, 1952.

5. Ferri, Antonio, and Nucci, Louis: The Origin of Aerodynamic Instability of Supersonic Inlets at Subcritical Conditions. NACA RM L50K30, 1951.

6. Schueller, Carl F., and Esenwein, Fred T.: Analytical and Experimental Investigation of Inlet-Engine Matching for Turbojet-Powered Aircraft at Mach Numbers up to 2.0. NACA RM E51K20, 1952.

[redacted]

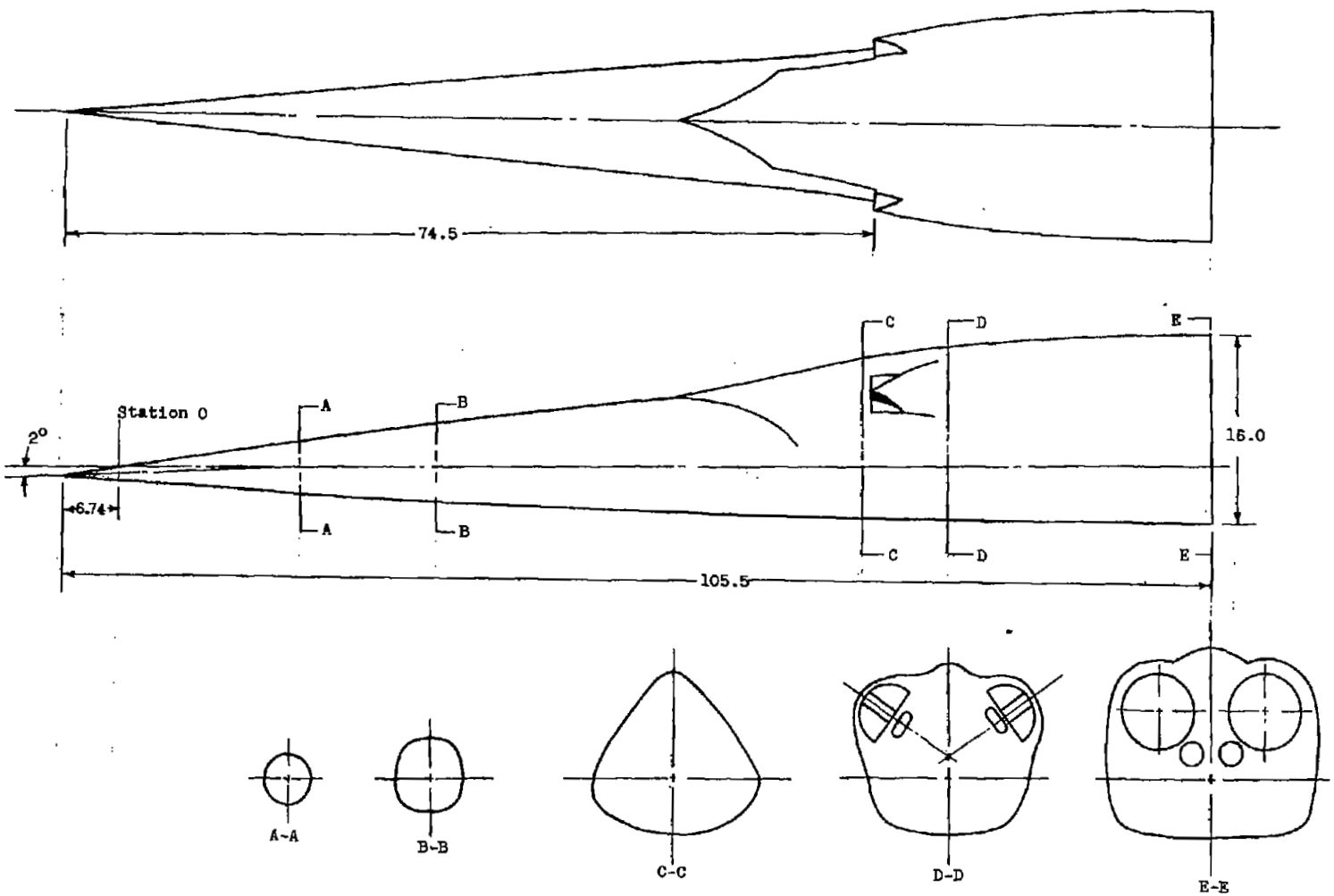

Figure 1. - Sketch of forward part of fuselage of a supersonic airplane showing typical model cross sections. (All linear dimensions in inches.)

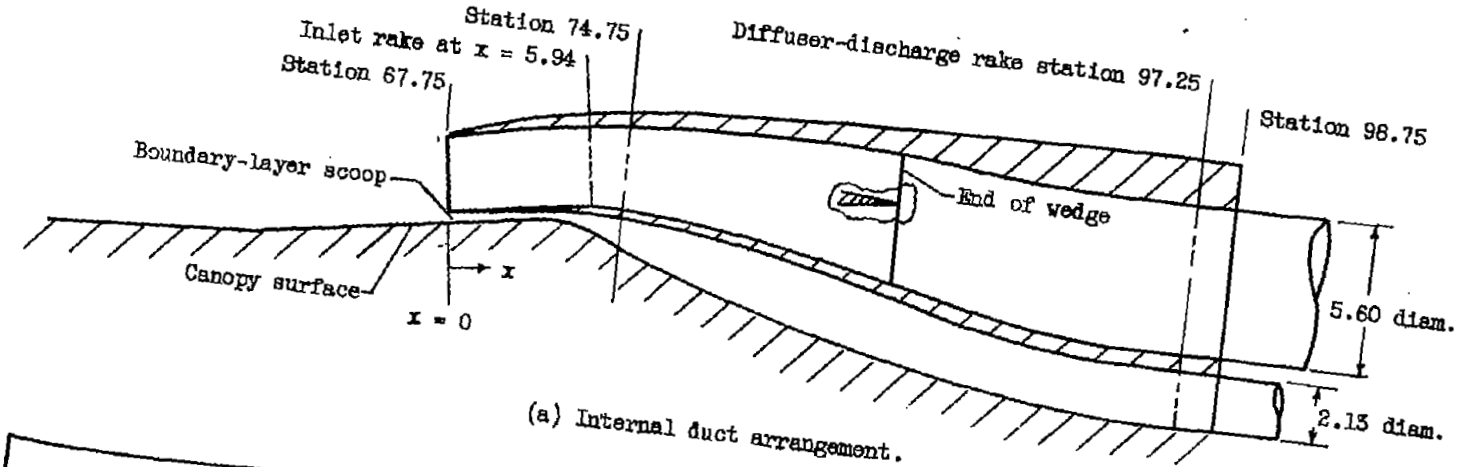

(a) Internal duct arrangement.

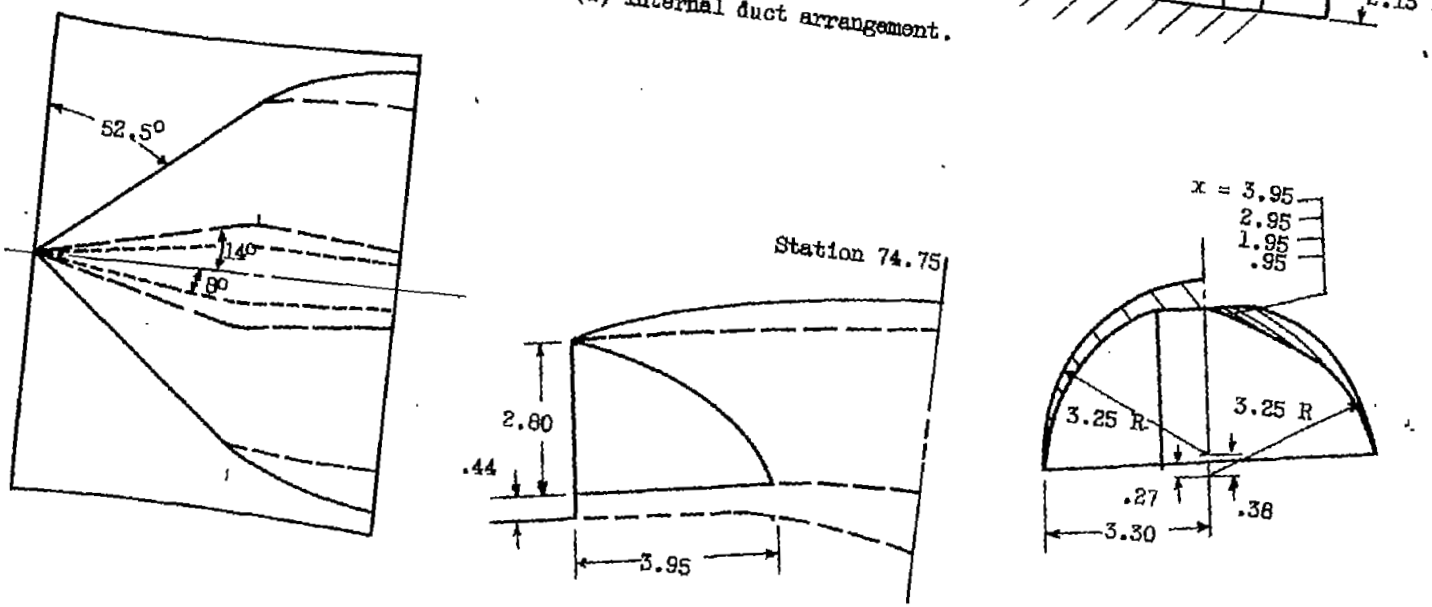

(b) Details of normal-wedge inlets.

Figure 2. - Sectional view of internal duct arrangement and details of normal-wedge inlets. (All linear dimensions in inches.)

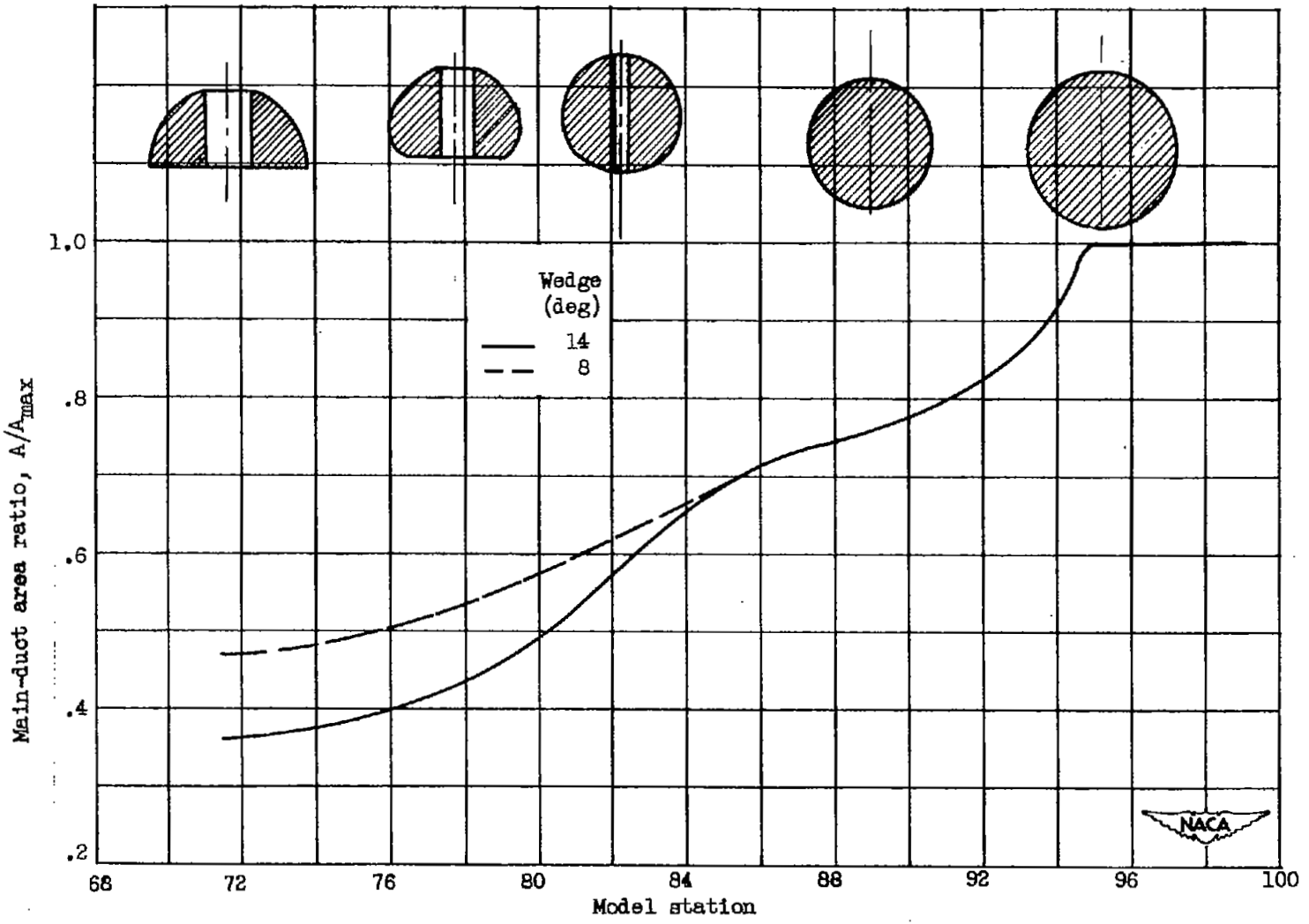

Figure 3. - Diffuser area variation for 14°- and 8°-wedge inlets with representative duct cross sections for 14°-wedge configuration.

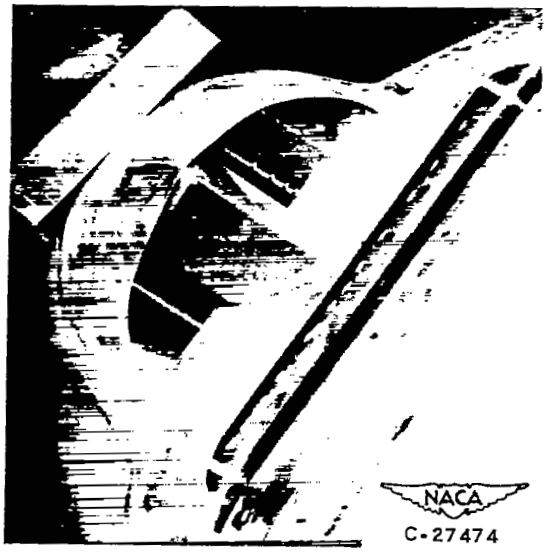

(a) Boundary-layer scoop with sides.

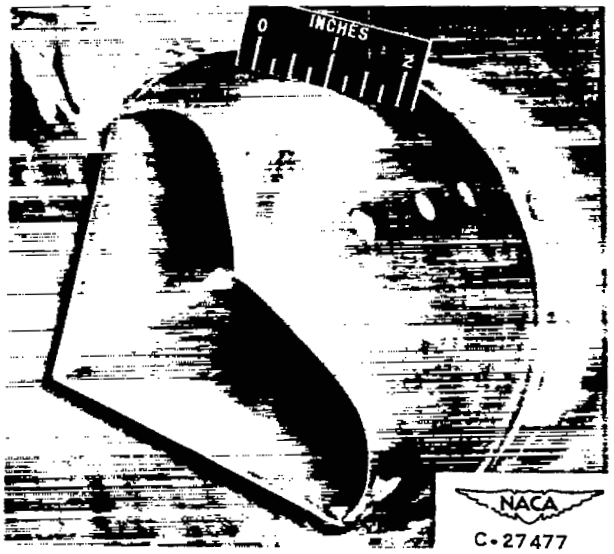

(c) Boundary-layer scoop with swept splitter plate.

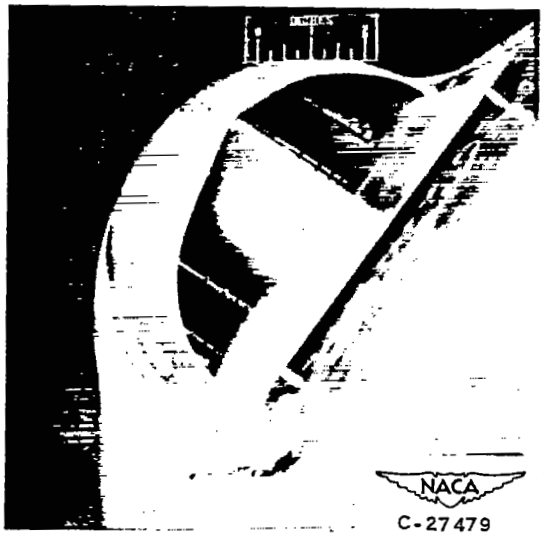

(b) Boundary-layer scoop with sides removed.

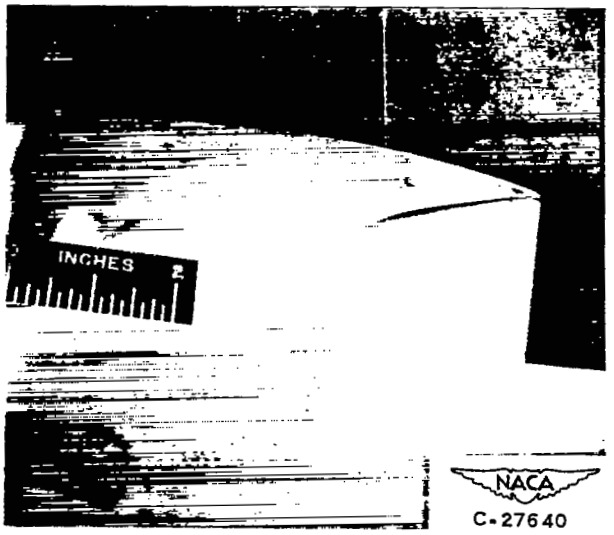

(d) Boundary-layer scoop faired into canopy.

Figure 4. - Photographs of three ram-type boundary-layer scoops and faired-canopy configuration investigated with normal-wedge inlets.

[redacted]

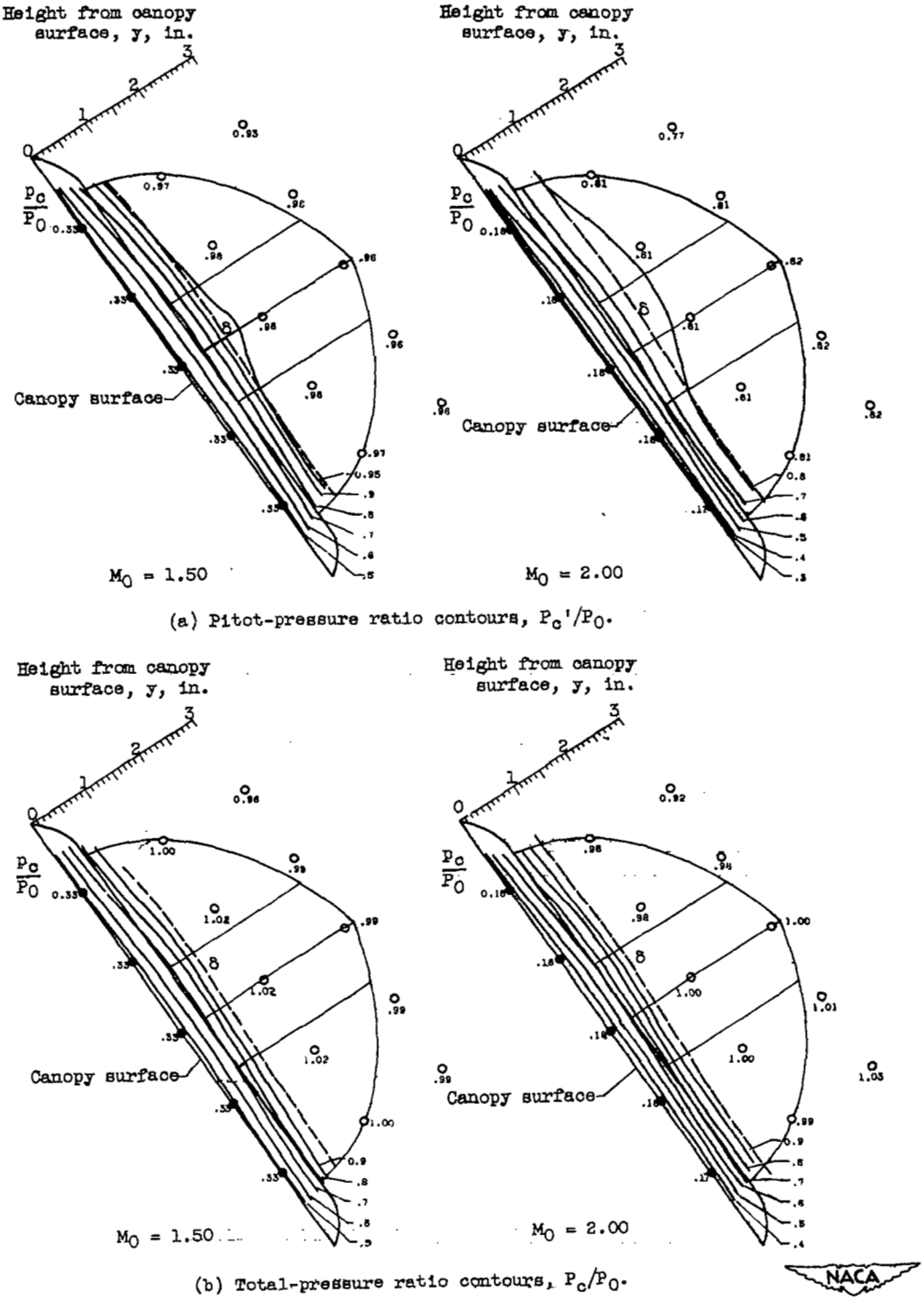

(a) Pitot-pressure ratio contours, P_c'/P_0.

(b) Total-pressure ratio contours, P_c/P_0.

Figure 5. - Flow survey ahead of inlets for cruise angle of attack ($\alpha = 3^\circ$) at free-stream Mach numbers of 1.50 and 2.00. Survey station, 67.5.

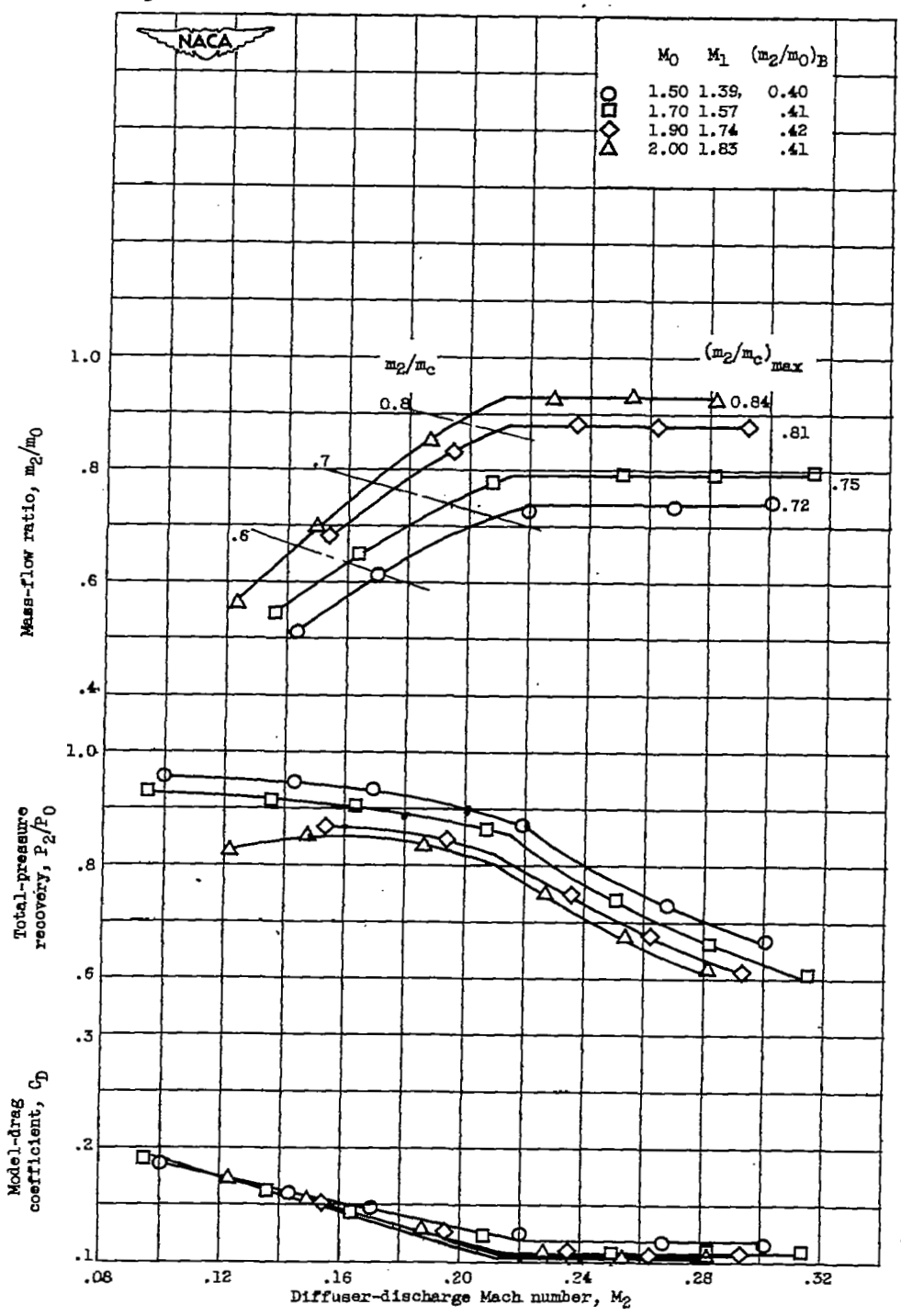

(a) 14°-wedge inlet utilizing boundary-layer scoop with sides; h/δ, 0.55; rated boundary-layer bleed flow.

Figure 6. - Characteristics of wedge inlets at Mach numbers from 1.50 to 2.00. Cruise angle of attack (α = 3°).

[redacted]

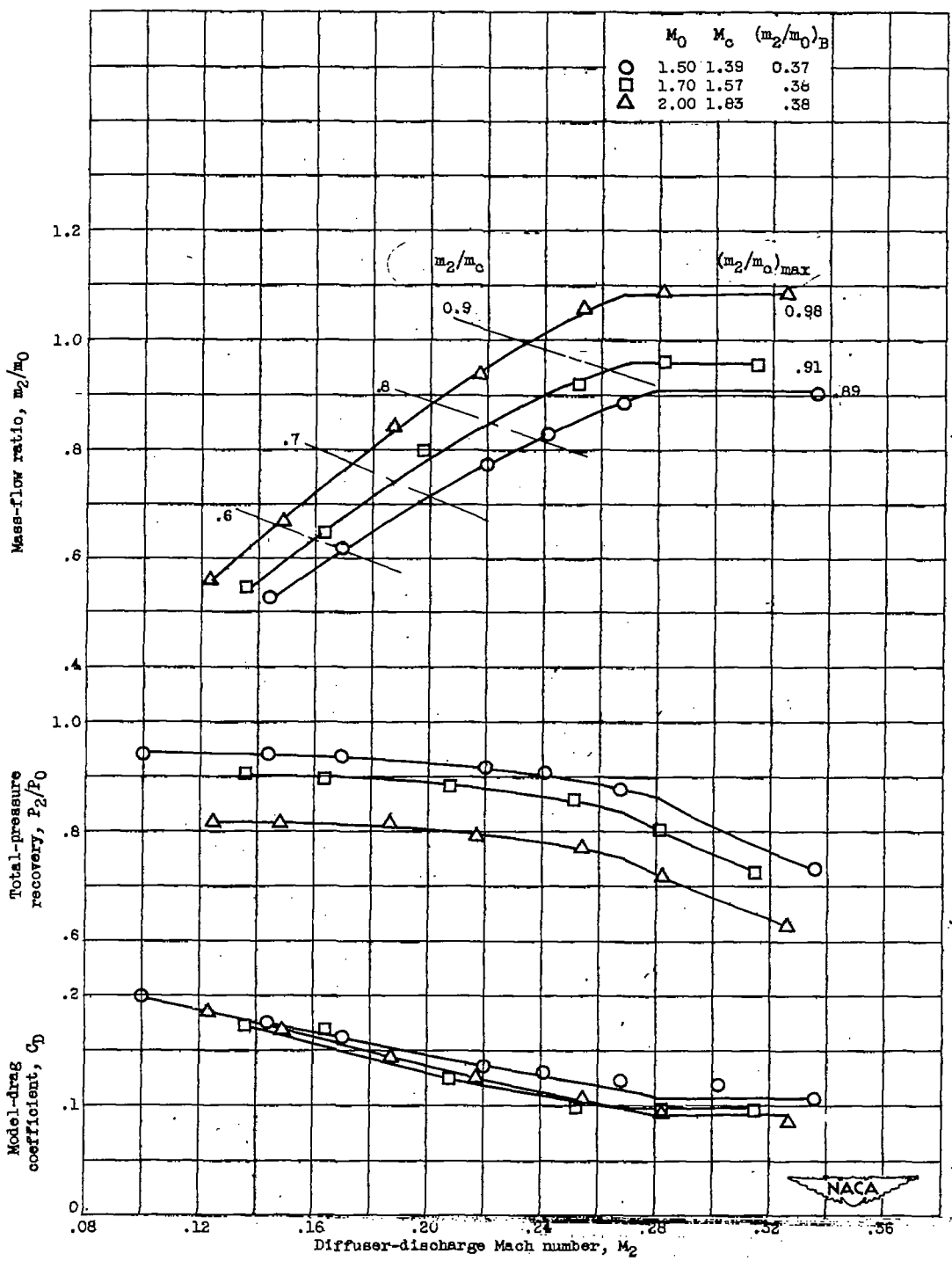

(b) 8°-wedge inlet utilizing boundary-layer scoop with sides; h/8, 0.55; rated boundary-layer bleed flow.

Figure 6. - Continued. Characteristics of wedge inlets at Mach numbers from 1.50 to 2.00. Cruise angle of attack (α = 3°).

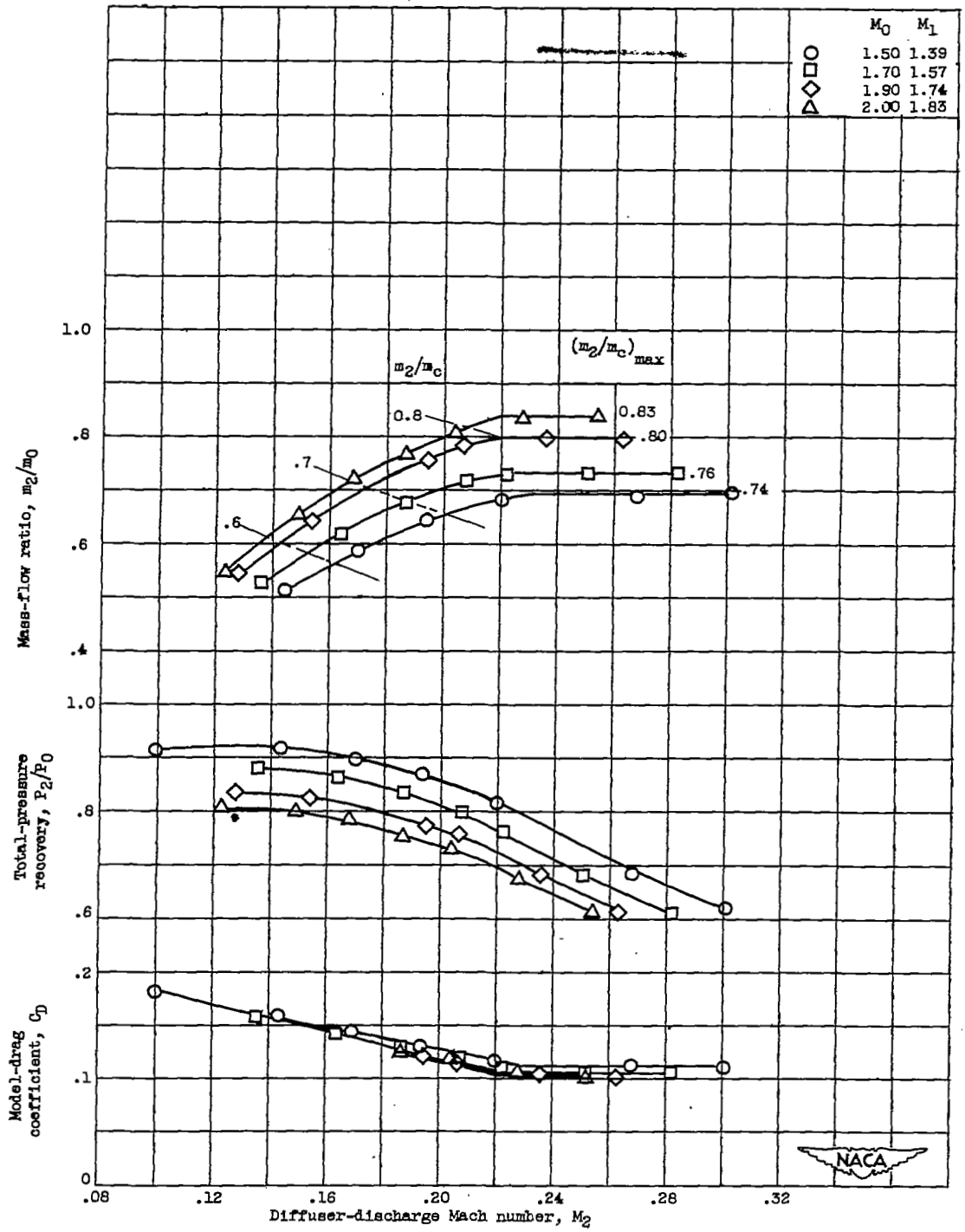

(c) 14°-wedge inlet with boundary-layer scoop faired into canopy; h/δ, 0; zero boundary-layer bleed flow.

Figure 6. - Concluded. Characteristics of wedge inlets at Mach numbers from 1.50 to 2.00. Cruise angle of attack ($\alpha = 3^\circ$).

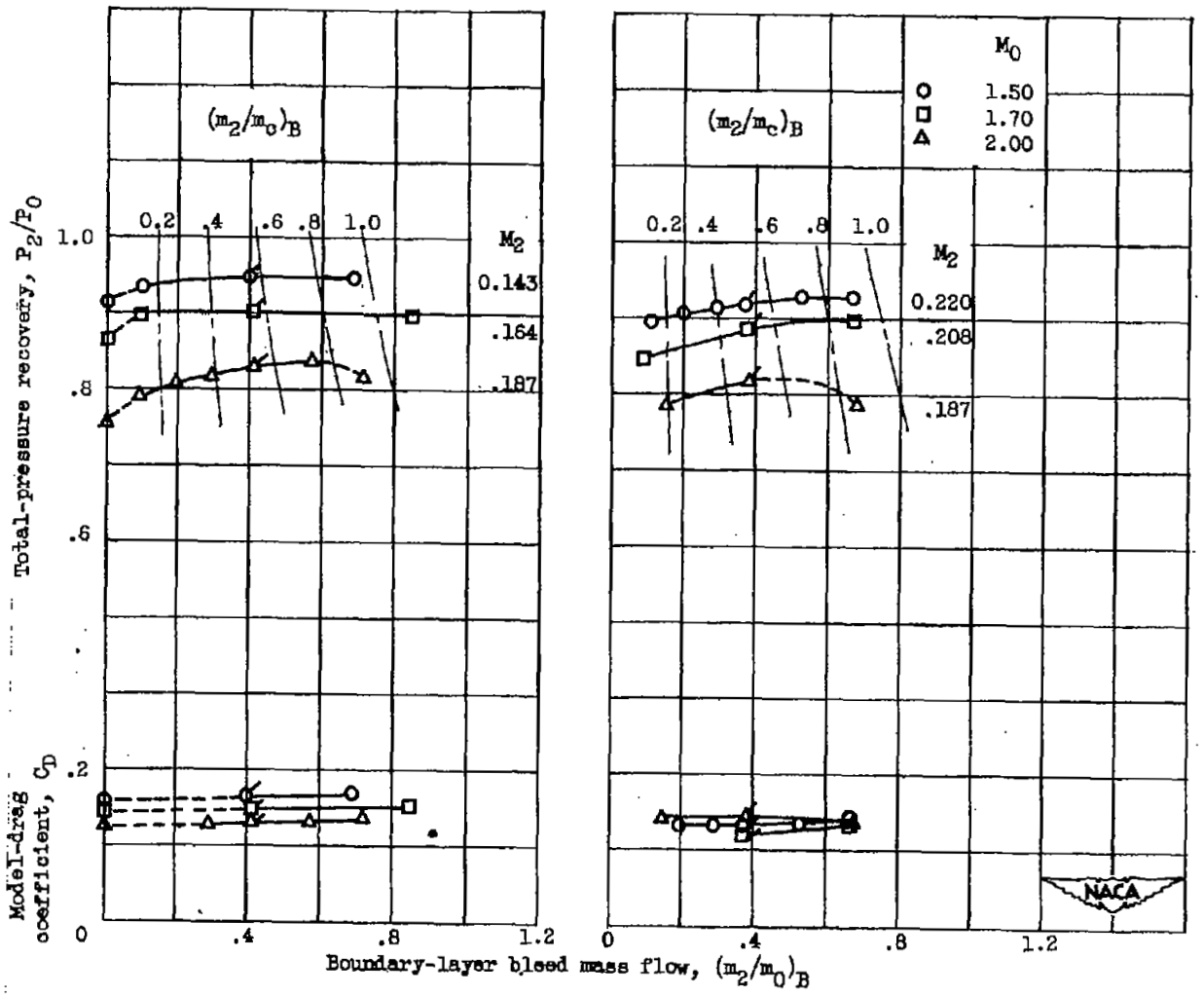

(a) 14°-wedge inlet; h/δ, 0.55. (b) 8°-wedge inlet; h/δ, 0.55.

Figure 7. - Variation of inlet performance characteristics for range of boundary-layer bleed mass flows at several free-stream Mach numbers. Cruise angle of attack ($\alpha = 3^\circ$).

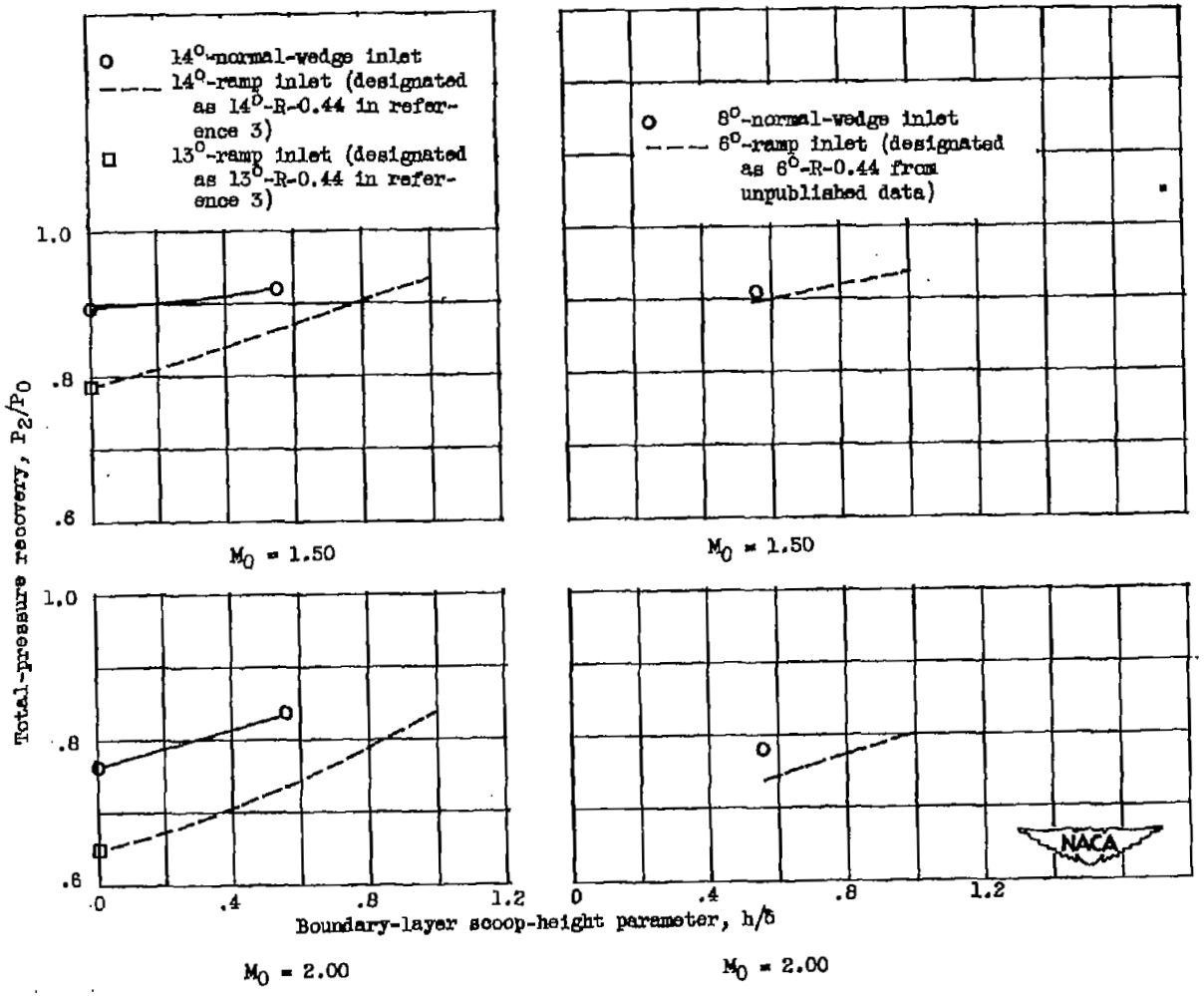

(a) 14°-normal-wedge inlet, 14°-ramp inlet, and 13°-ramp inlet.

(b) 8°-normal-wedge inlet and 6°-ramp inlet.

Figure 8. - Variation of inlet pressure recovery characteristics at maximum thrust minus drag over range of scoop-height to boundary-layer-thickness ratios at Mach numbers of 1.50 and 2.00. Cruise angle of attack (α = 5°); rated boundary-layer bleed flow.

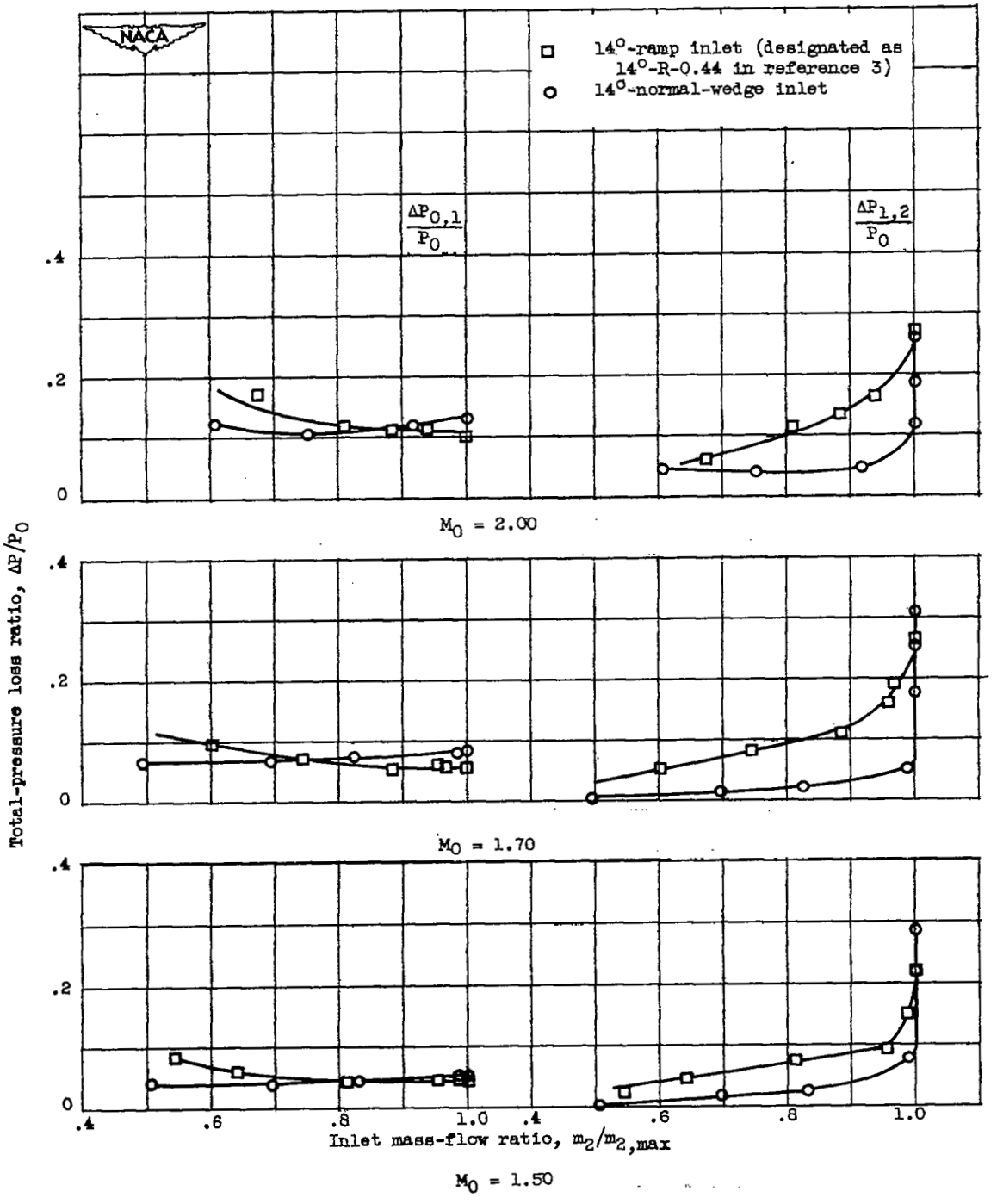

(a) 14°-wedge inlet; h/δ, 0.55; rated boundary-layer bleed flow.

Figure 9. - Components of total-pressure losses at several free-stream Mach numbers. Cruise angle of attack ($\alpha = 3^\circ$).

[redacted]

2528

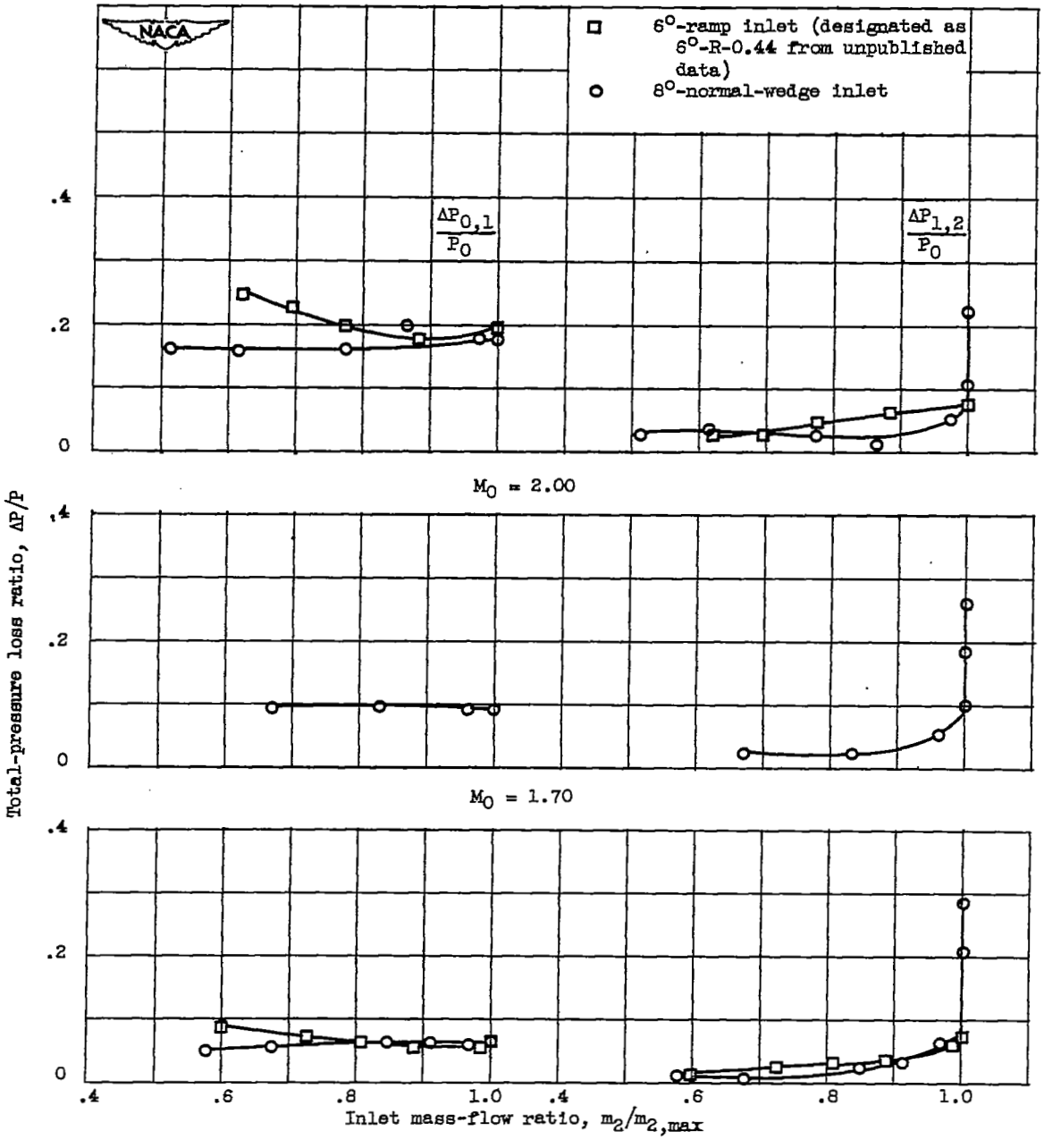

(b) 8°-wedge inlet; h/δ, 0.55; rated boundary-layer bleed flow.

Figure 9. - Continued. Components of total-pressure losses at several free-stream Mach numbers. Cruise angle of attack (α = 3°).

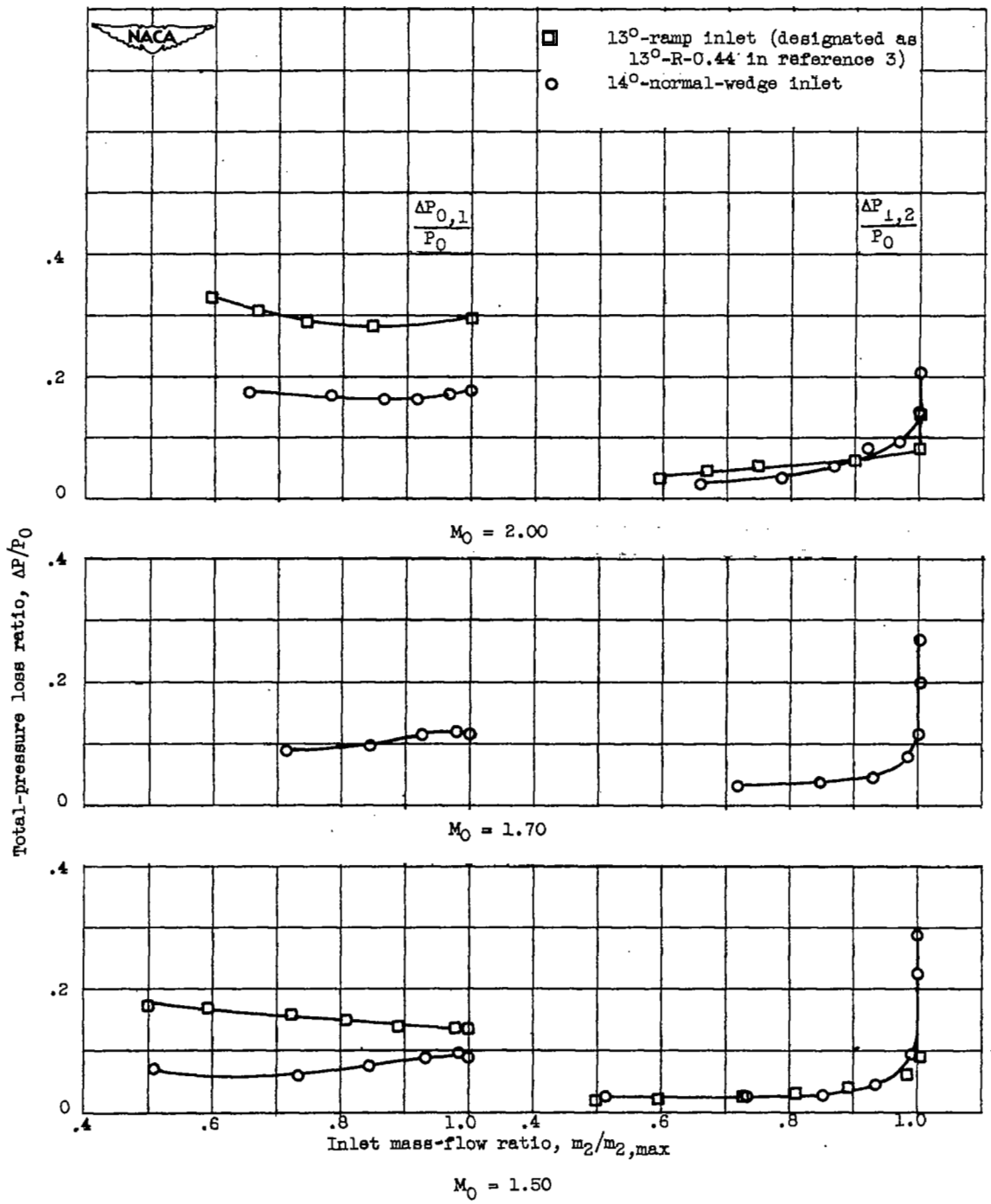

2528

(c) 14°-wedge inlet, h/δ, 0; zero boundary-layer bleed flow.

Figure 9. - Concluded. Components of total-pressure losses at several free-stream Mach numbers. Cruise angle of attack (α = 3°).

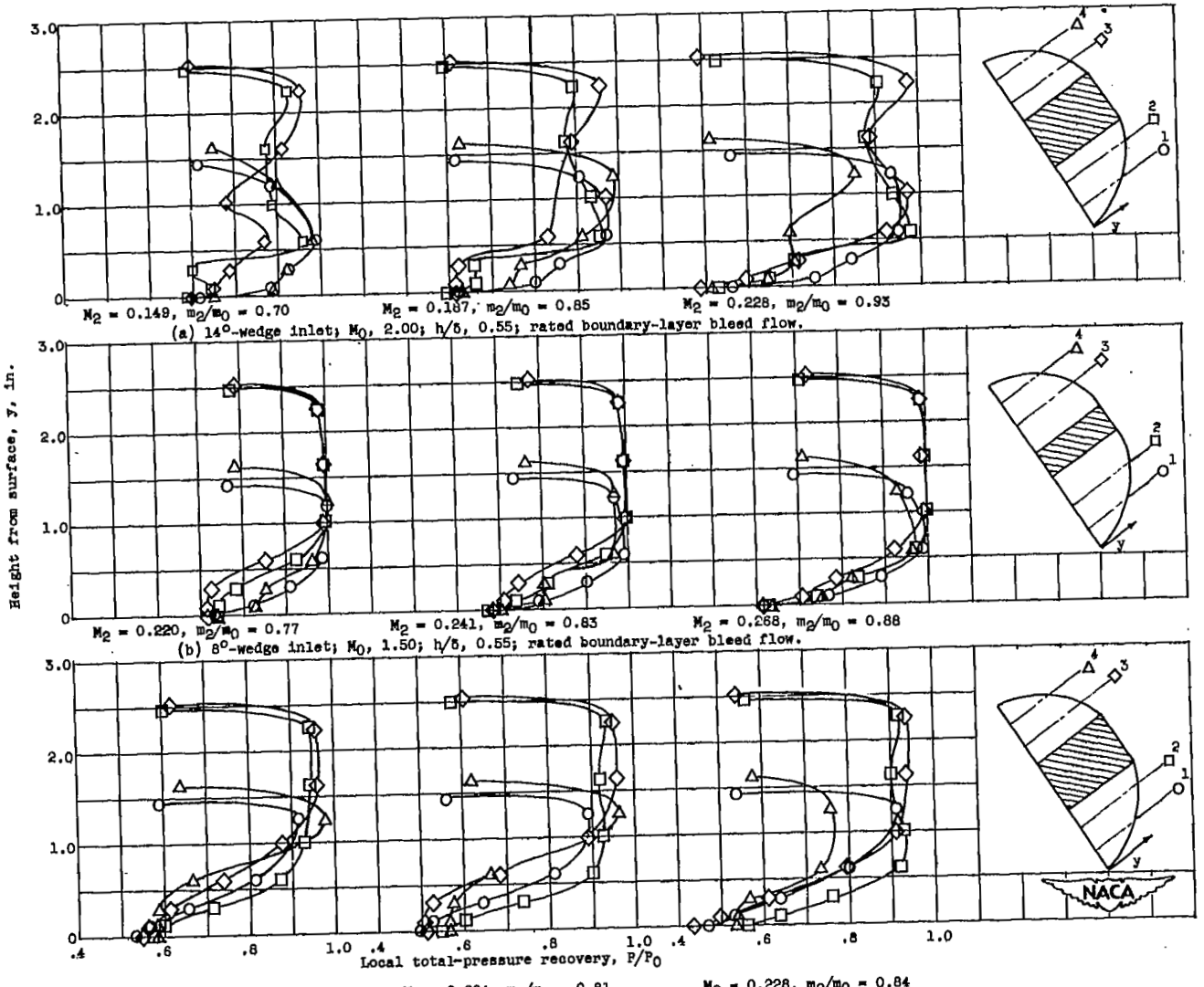

$M_2 = 0.149$, $m_2/m_0 = 0.70$ $M_2 = 0.187$, $m_2/m_0 = 0.85$ $M_2 = 0.228$, $m_2/m_0 = 0.93$

(a) 14°-wedge inlet; M_0, 2.00; h/5, 0.55; rated boundary-layer bleed flow.

$M_2 = 0.220$, $m_2/m_0 = 0.77$ $M_2 = 0.241$, $m_2/m_0 = 0.83$ $M_2 = 0.268$, $m_2/m_0 = 0.88$

(b) 8°-wedge inlet; M_0, 1.50; h/5, 0.55; rated boundary-layer bleed flow.

$M_2 = 0.187$, $m_2/m_0 = 0.77$ $M_2 = 0.204$, $m_2/m_0 = 0.81$ $M_2 = 0.228$, $m_2/m_0 = 0.84$

(c) 14°-wedge inlet; M_0, 2.00; h/5, 0; zero boundary-layer bleed flow.

Figure 10. - Typical total-pressure profiles at inlet (station, x = 5.94) for three inlet configurations. Cruise angle of attack ($\alpha = 3°$).

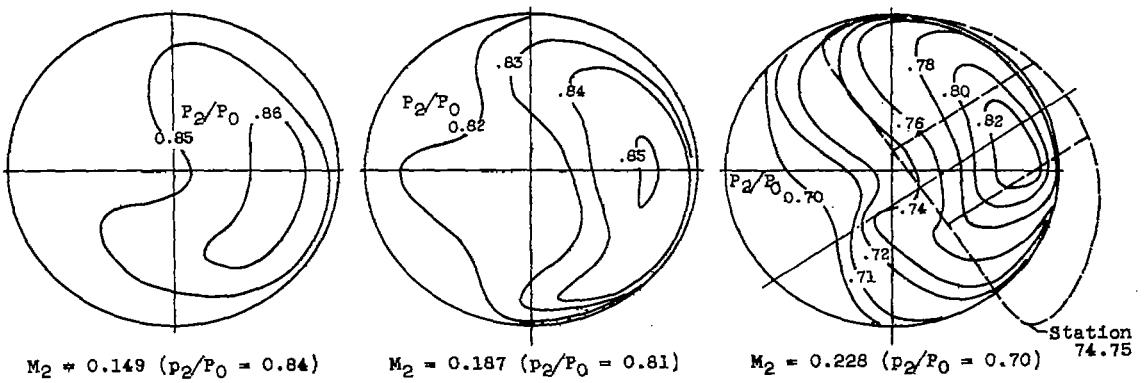

$M_2 = 0.149$ ($p_2/P_0 = 0.84$) $M_2 = 0.187$ ($p_2/P_0 = 0.81$) $M_2 = 0.228$ ($p_2/P_0 = 0.70$)

(a) 14°-wedge inlet; M_0, 2.00; h/δ, 0.55; rated boundary-layer bleed flow.

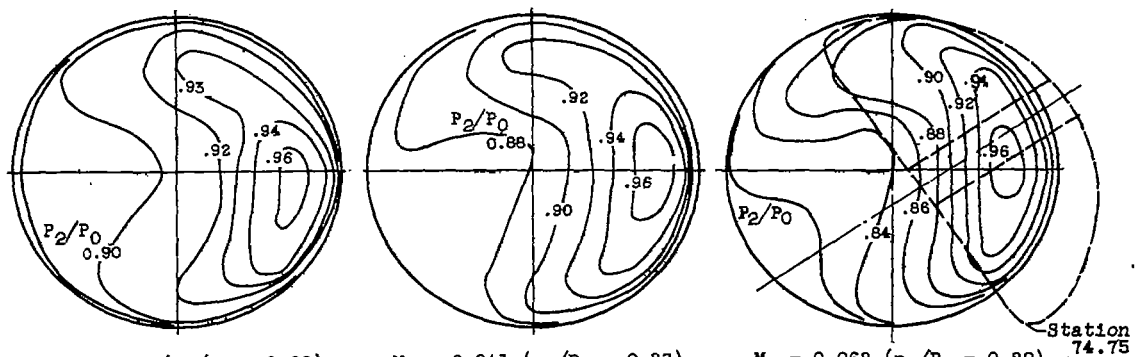

$M_2 = 0.220$ ($p_2/P_0 = 0.88$) $M_2 = 0.241$ ($p_2/P_0 = 0.87$) $M_2 = 0.268$ ($p_2/P_0 = 0.82$)

(b) 8°-wedge inlet; M_0, 1.50; h/δ, 0.55; rated boundary-layer bleed flow.

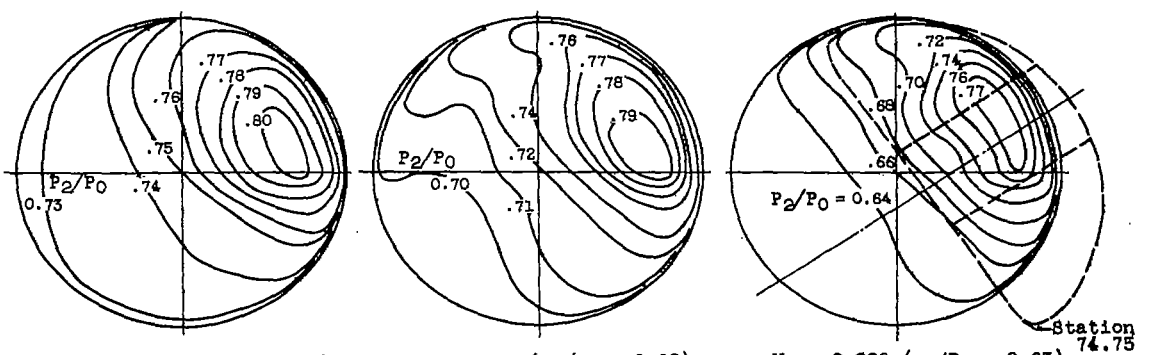

$M_2 = 0.187$ ($p_2/P_0 = 0.72$) $M_2 = 0.204$ ($p_2/P_0 = 0.69$) $M_2 = 0.228$ ($p_2/P_0 = 0.63$)

(c) 14°-wedge inlet; M_0, 2.00; h/δ, 0; zero boundary-layer bleed flow.

NACA

Figure 11. - Typical total-pressure contours at diffuser discharge (station 97.25). Cruise angle of attack ($\alpha = 3°$).

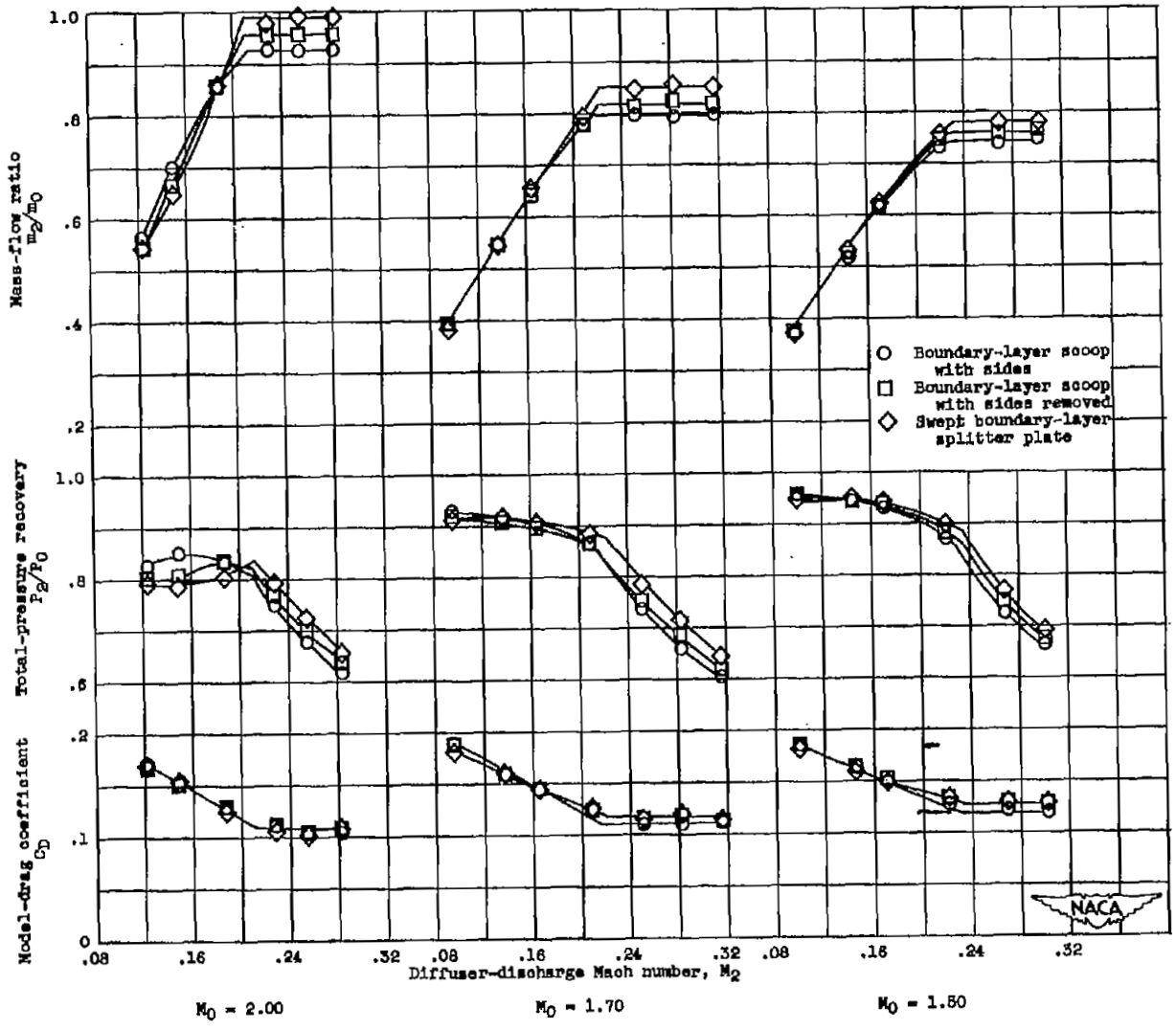

(a) 14°-wedge inlet.

Figure 12. - Comparison of performance characteristics for several boundary-layer scoop configurations at several free-stream Mach numbers. Cruise angle of attack (α = 3°); h/δ, 0.55; rated boundary-layer bleed flow.

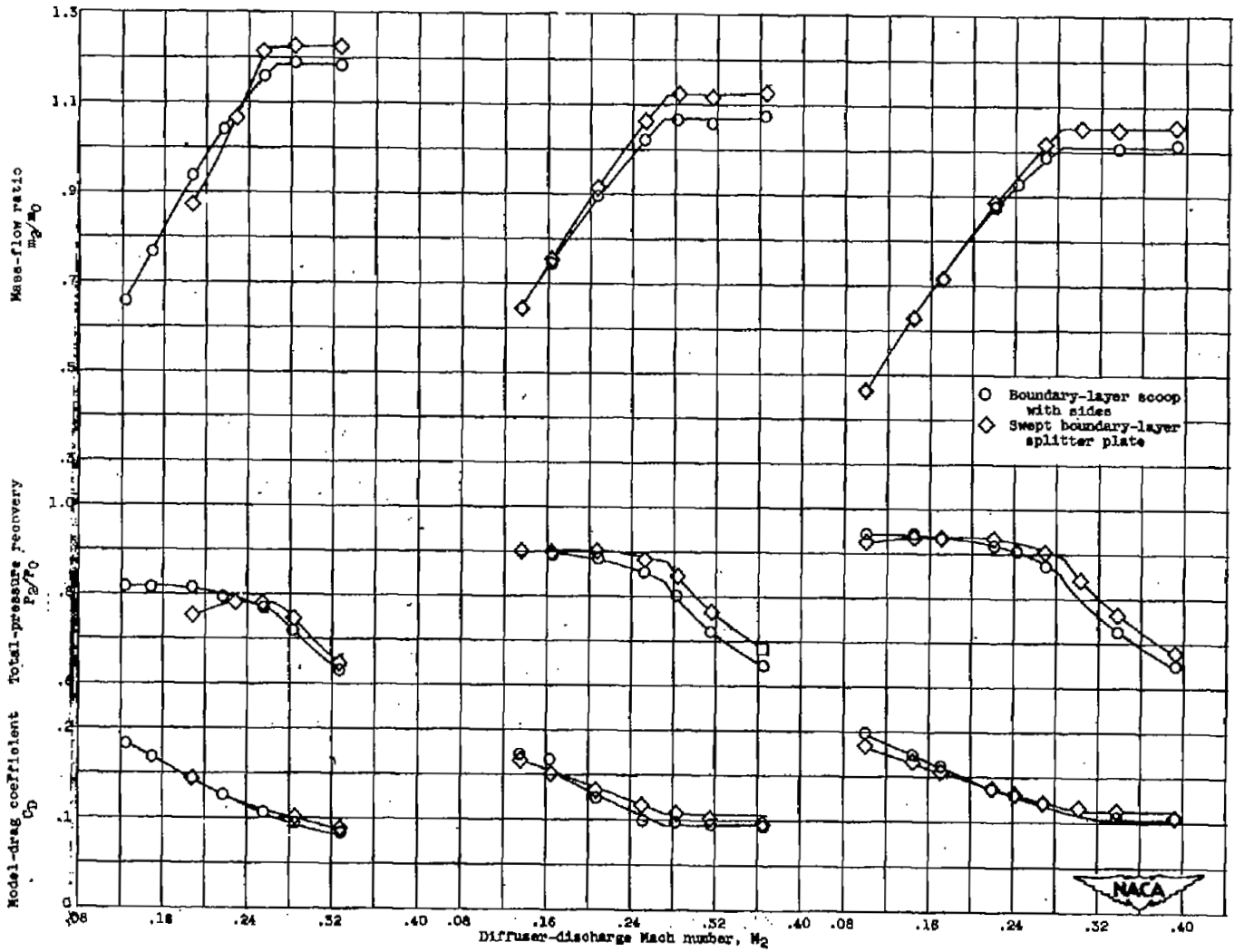

(b) 8°-wedge inlet.

Figure 12. - Concluded. Comparison of performance characteristics for several boundary-layer scoop configurations at several free-stream Mach numbers. Cruise angle of attack ($\alpha = 5^\circ$); h/δ, 0.55; rated boundary-layer bleed flow.

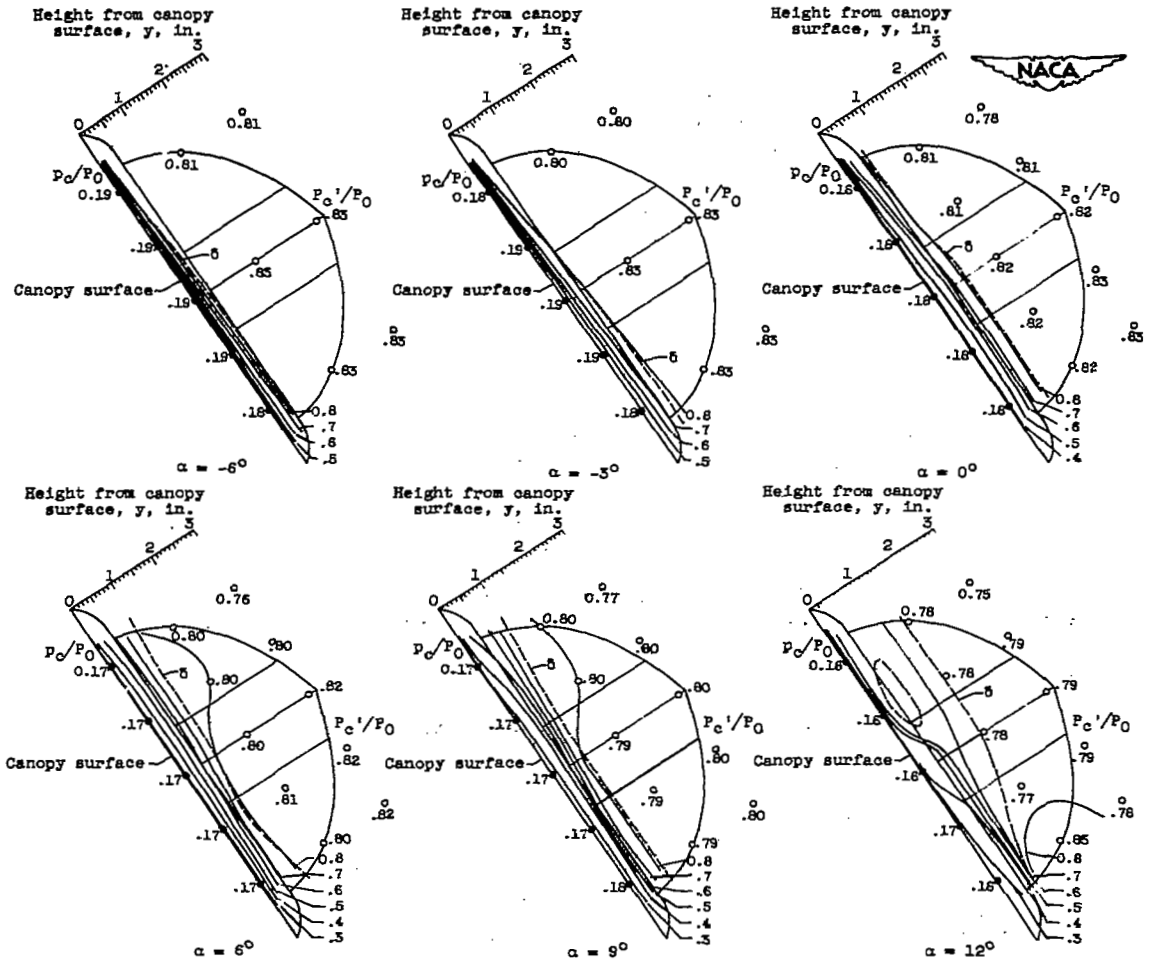

Figure 13. - Pitot-pressure ratio contours, P_c'/P_0 of flow survey ahead of inlets for range of angles of attack from -6° to 12° at free-stream Mach number of 2.00. Survey station, 67.5.

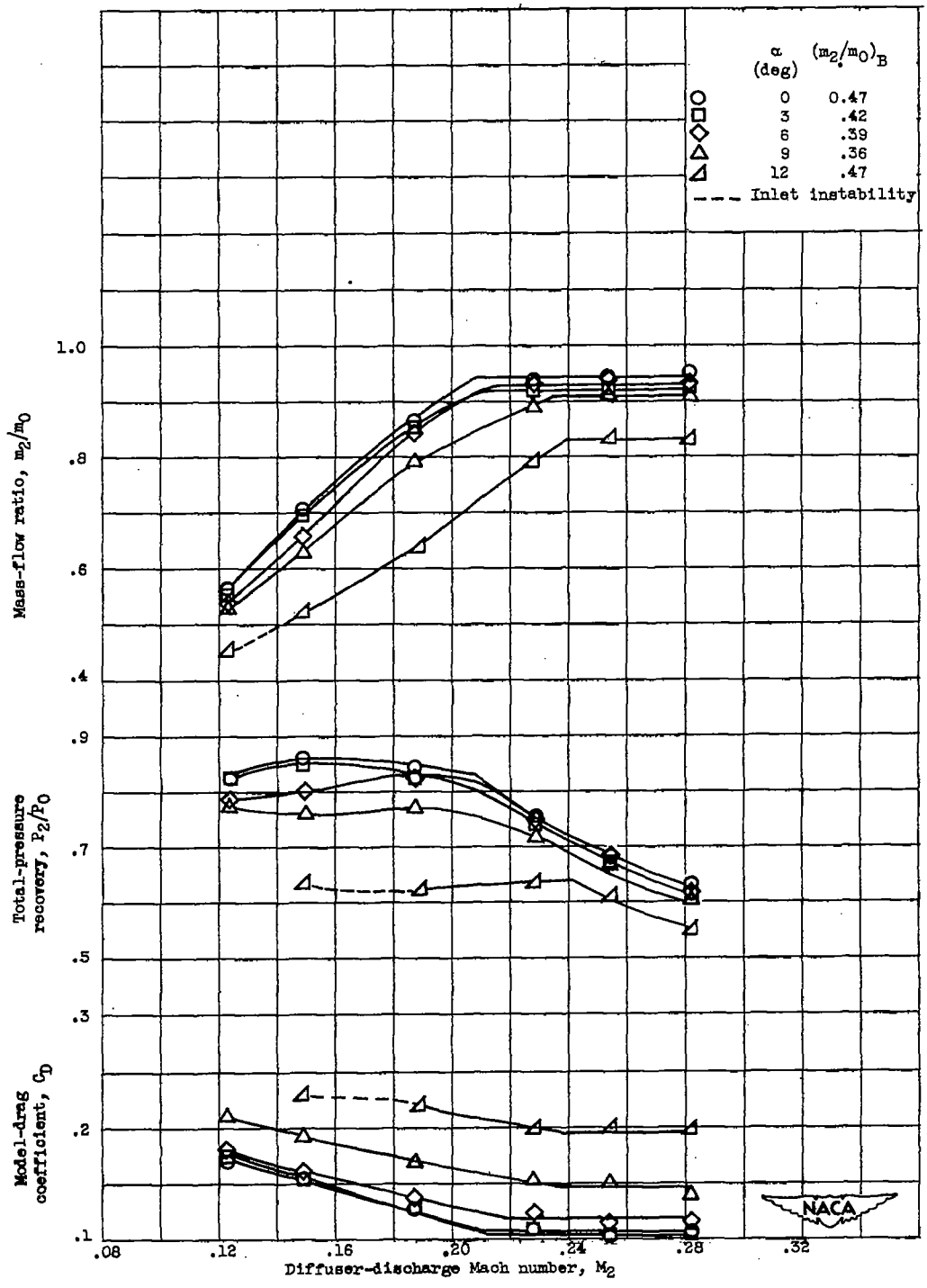

(a) 14°-wedge inlet utilizing boundary-layer scoop with sides; M_0, 2.00; h/δ, 0.55; rated boundary-layer bleed flow.

Figure 14. - Characteristics of wedge inlets for range of angles of attack from 0° to 12°.

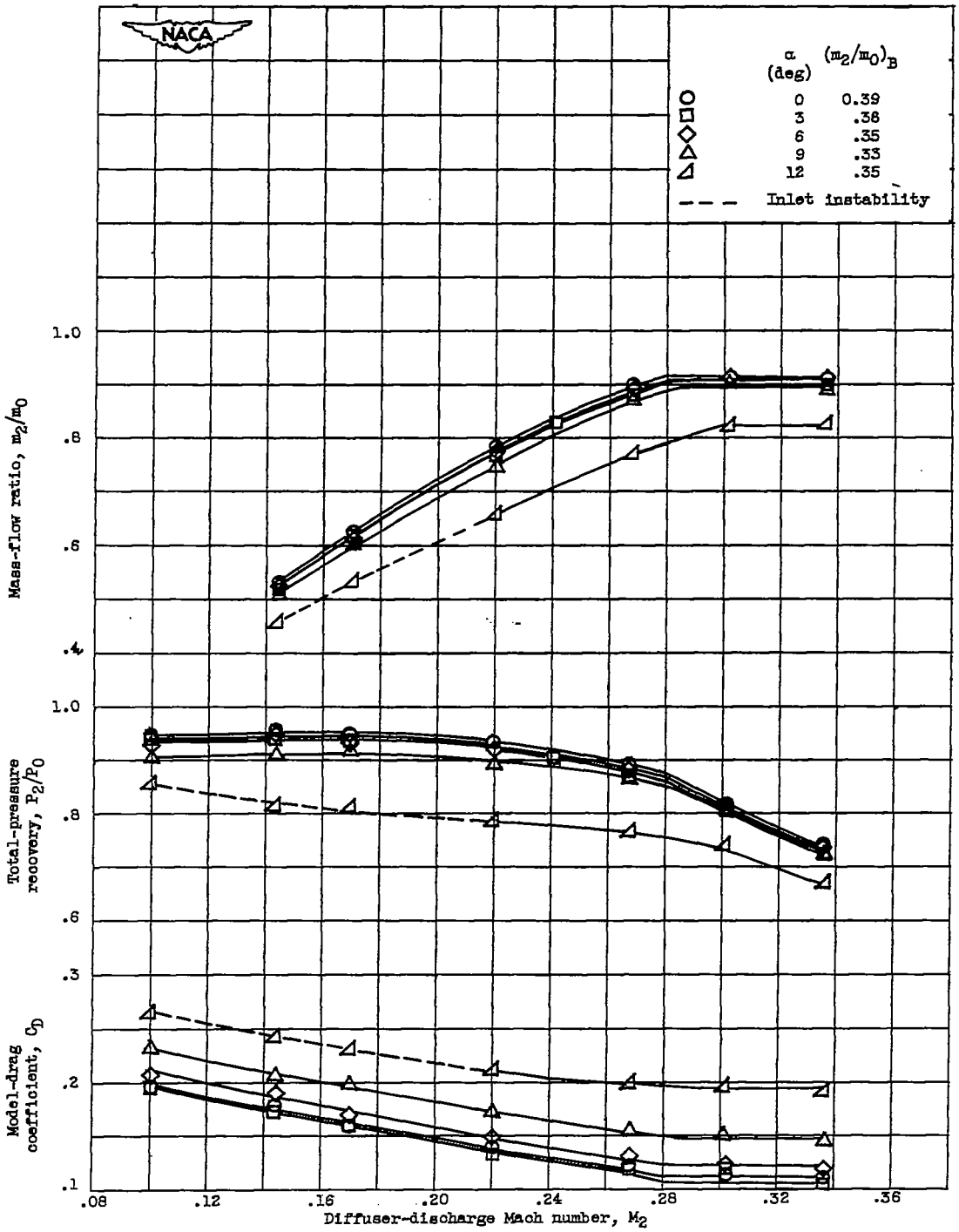

(b) 8°-wedge inlet utilizing boundary-layer scoop with sides; M_0, 1.50; h/δ, 0.55; rated boundary-layer bleed flow.

Figure 14. - Continued. Characteristics of wedge inlets for range of angles of attack from 0° to 12°.

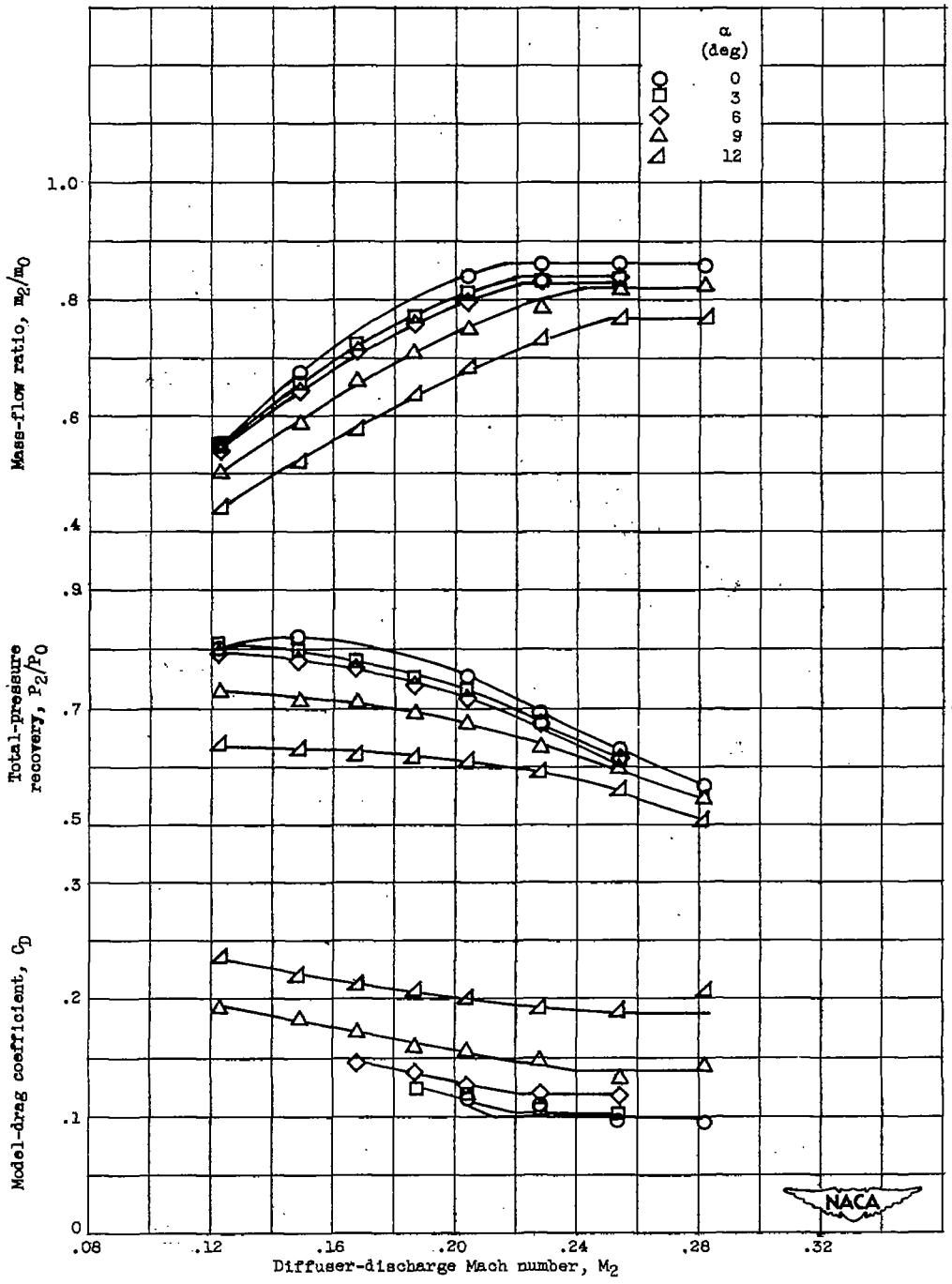

(c) 14°-wedge inlet with boundary-layer scoop faired into canopy; M_0, 2.00; h/δ, 0; zero boundary-layer bleed flow.

Figure 14. - Concluded. Characteristics of wedge inlets for range of angles of attack from 0° to 12°.

[redacted]

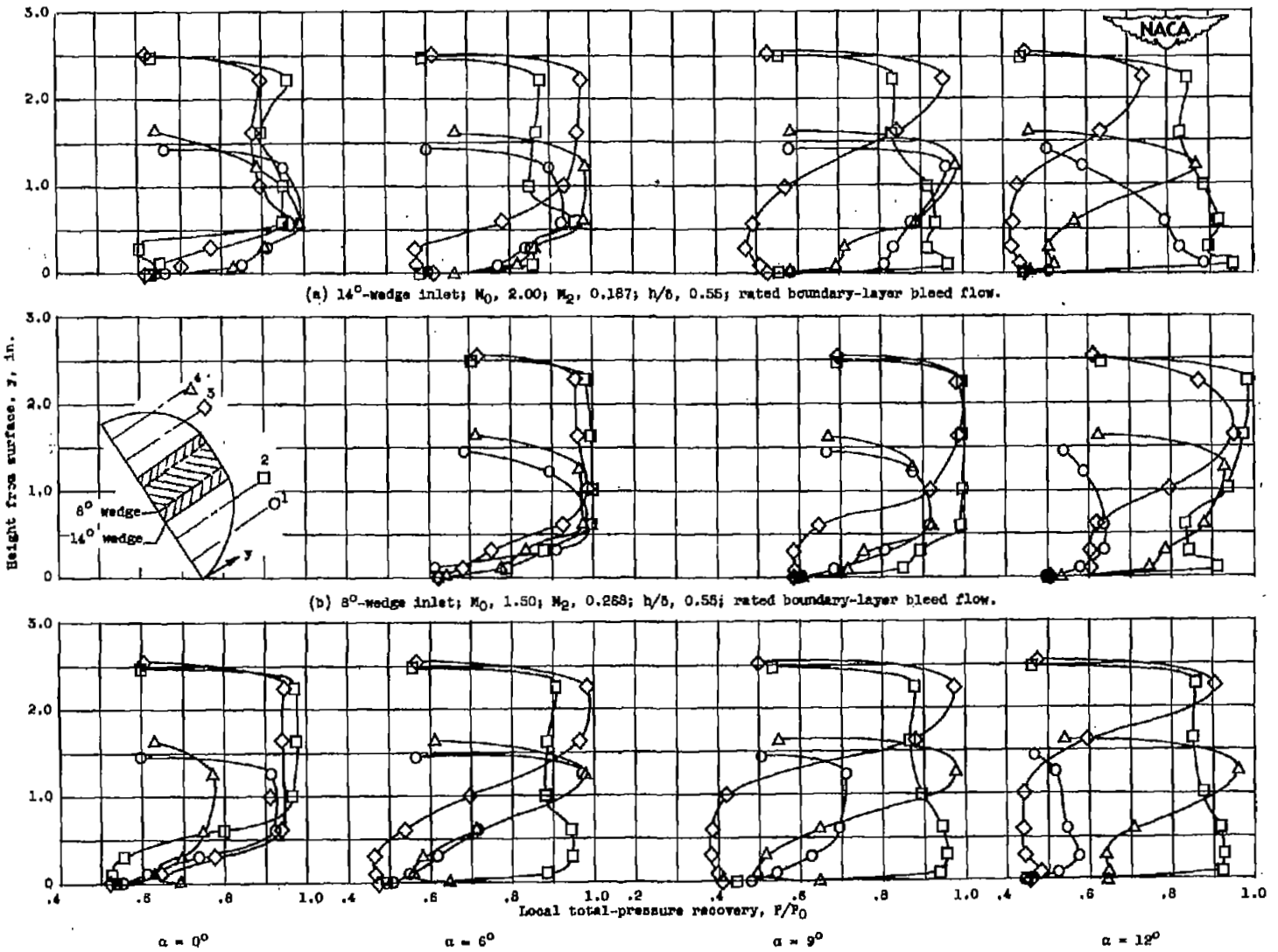

(a) 14°-wedge inlet; M_0, 2.00; M_2, 0.187; h/δ, 0.55; rated boundary-layer bleed flow.

(b) 8°-wedge inlet; M_0, 1.80; M_2, 0.268; h/δ, 0.55; rated boundary-layer bleed flow.

(c) 14°-wedge inlet; M_0, 2.00; M_2, 0.204; h/δ, 0; zero boundary-layer bleed flow.

Figure 15. - Typical total-pressure profiles at inlet (station, x = 5.94) for range of angles of attack from 0° to 12°.

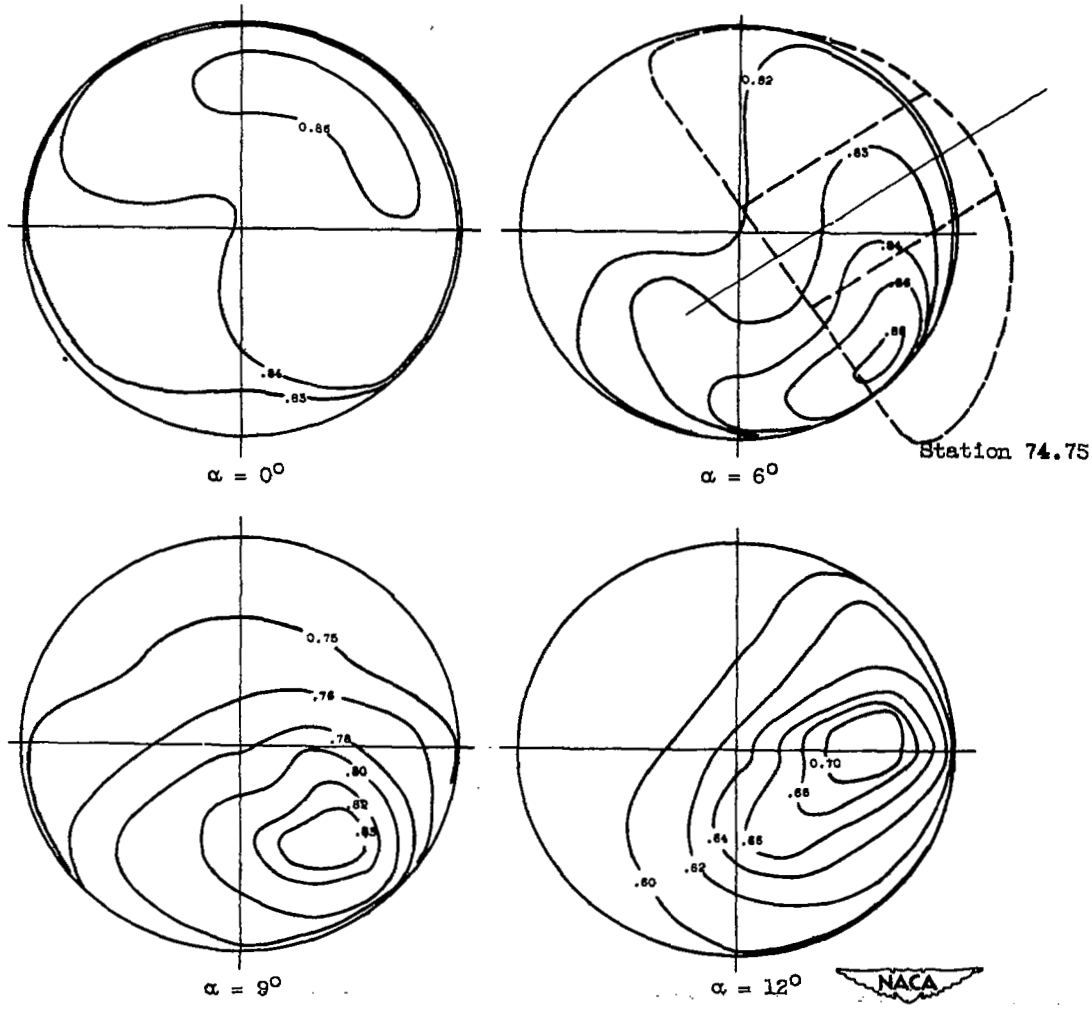

(a) 14°-wedge inlet; M_0, 2.00; M_2, 0.187; h/δ, 0.55; rated boundary-layer bleed flow.

Figure 16. - Typical total-pressure contours at diffuser discharge (station 97.25) for range of angles of attack from 0° to 12°.

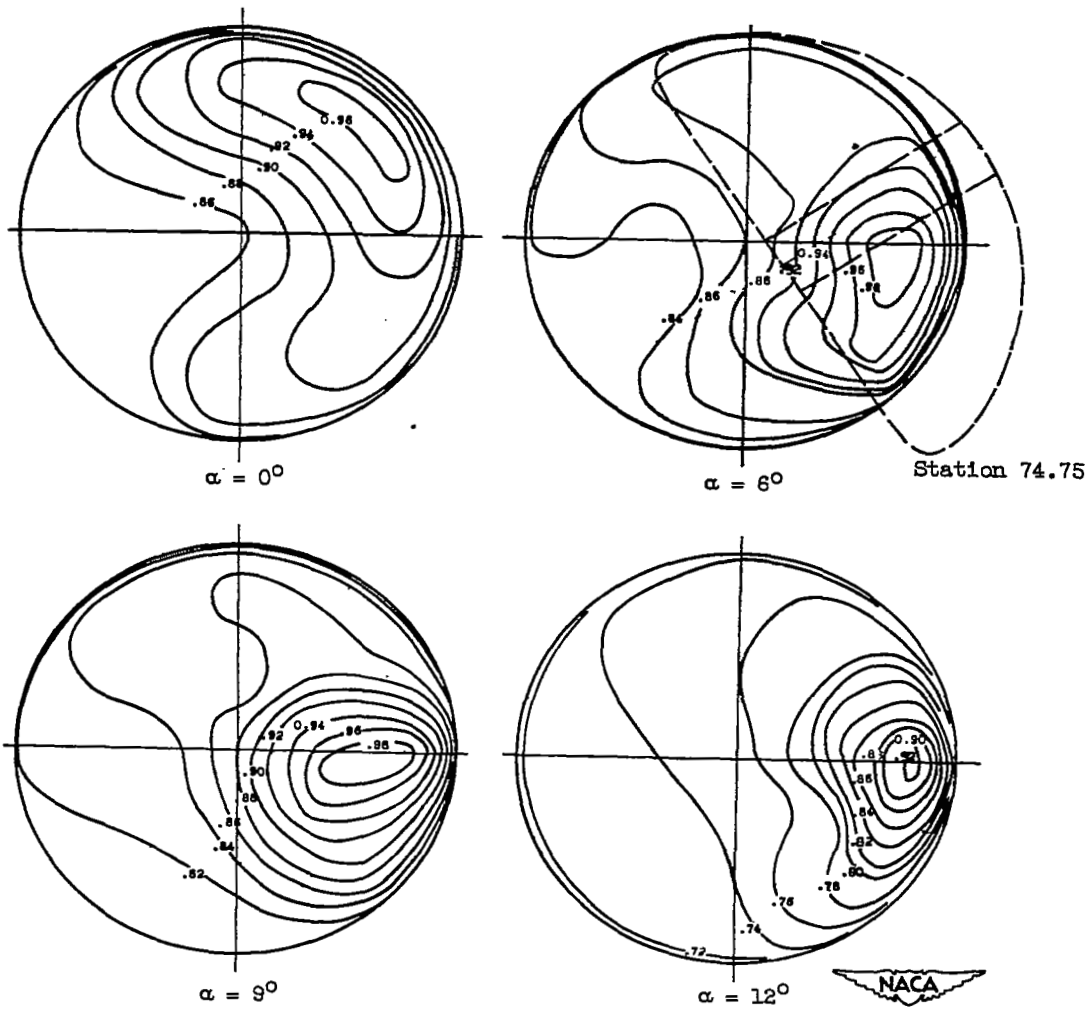

(b) 8°-wedge inlet; M_0, 1.50; M_2, 0.268; h/δ, 0.55; rated boundary-layer bleed flow.

Figure 16. - Continued. Typical total-pressure contours at diffuser discharge (station 97.25) for range of angles of attack from 0° to 12°.

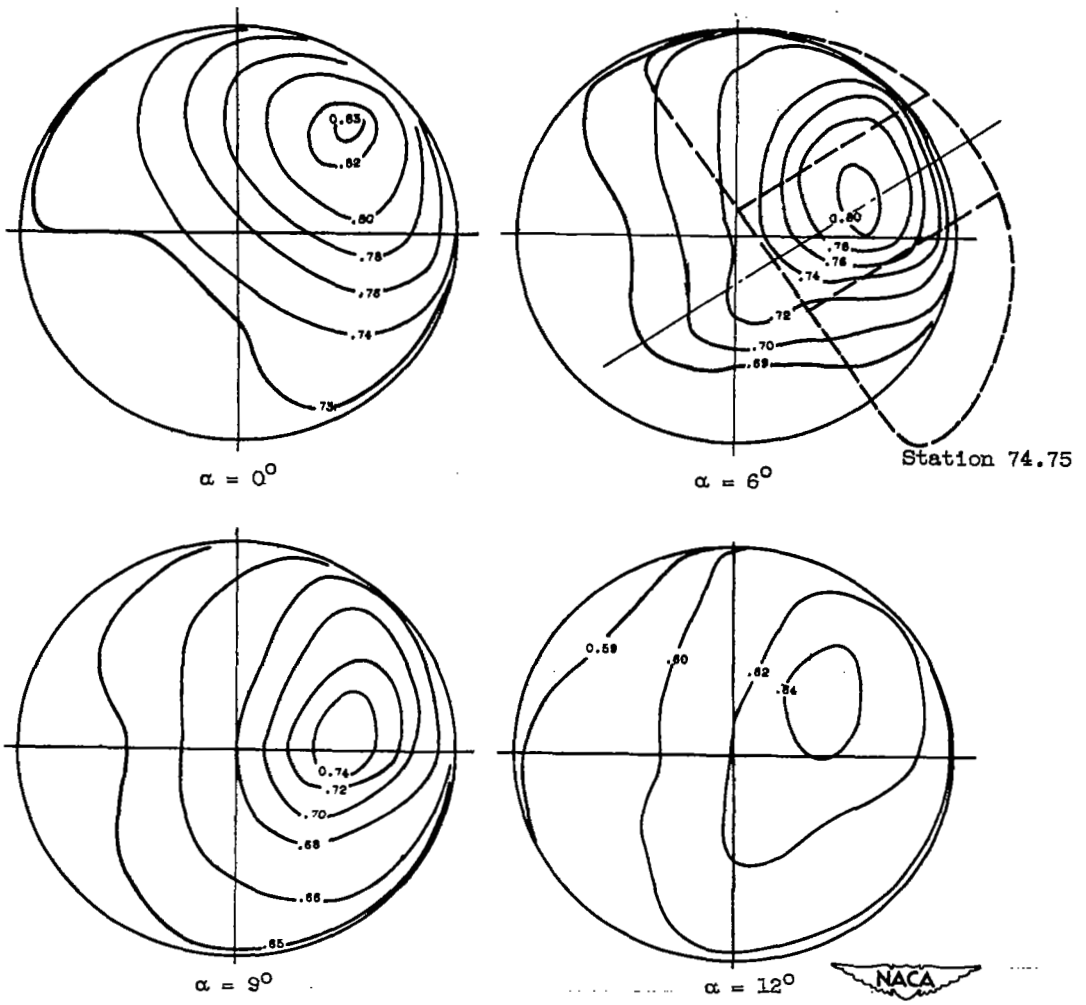

(c) 14°-wedge inlet; M_0, 2.00; M_2, 0.204; h/8, 0; zero boundary-layer bleed flow.

Figure 16. - Concluded. Typical total-pressure contours at diffuser discharge (station 97.25) for range of angles of attack from 0° to 12°.

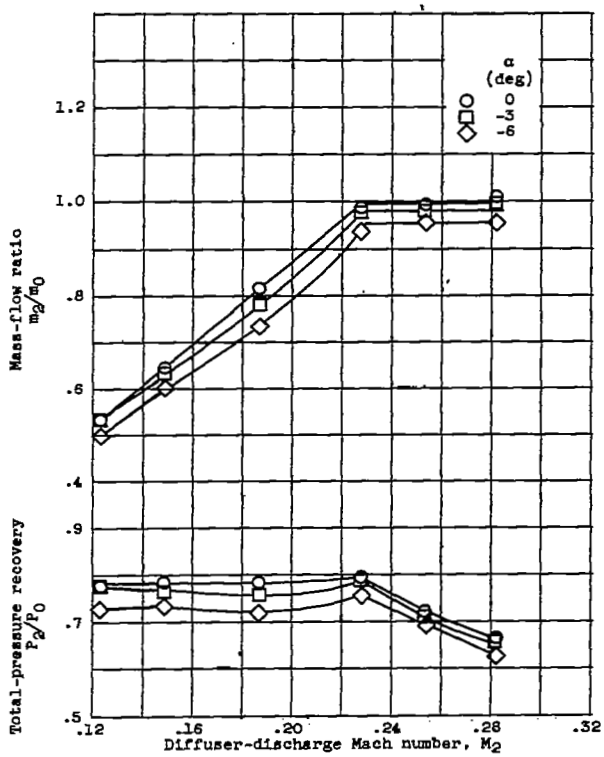

Figure 17. - Characteristics of 14°-wedge inlet with swept boundary-layer splitter plate for range of angles of attack from 0° to -6° at Mach number of 2.00.

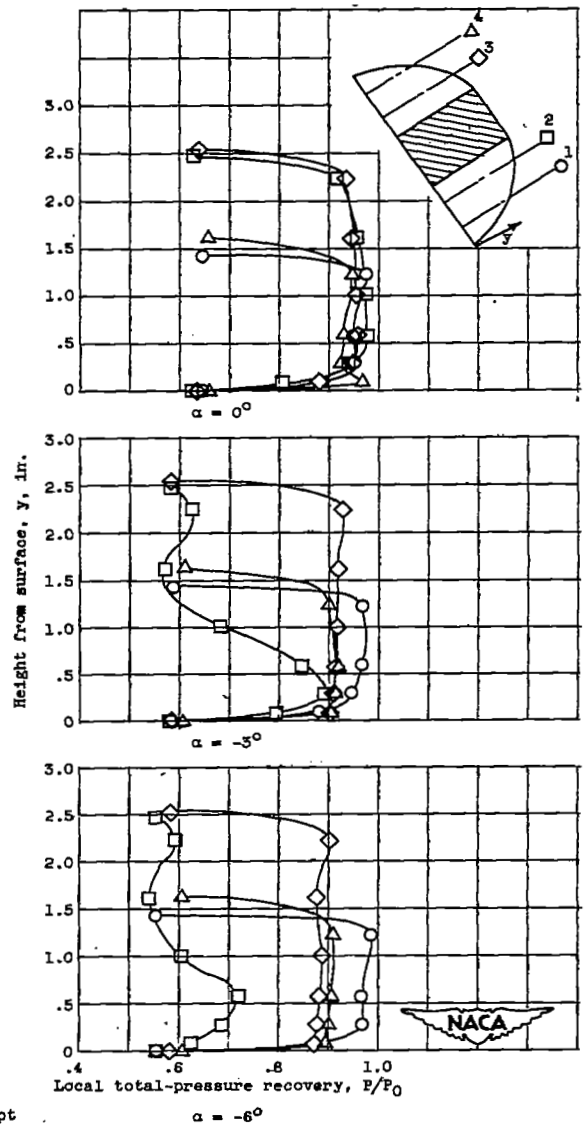

Figure 18. - Typical total-pressure profiles at inlet (station, x = 5.94) for 14°-wedge inlet with swept boundary-layer splitter plate at angles of attack from 0° to -6°. M_0, 2.00; h/δ, 0.55; rated boundary-layer bleed flow.

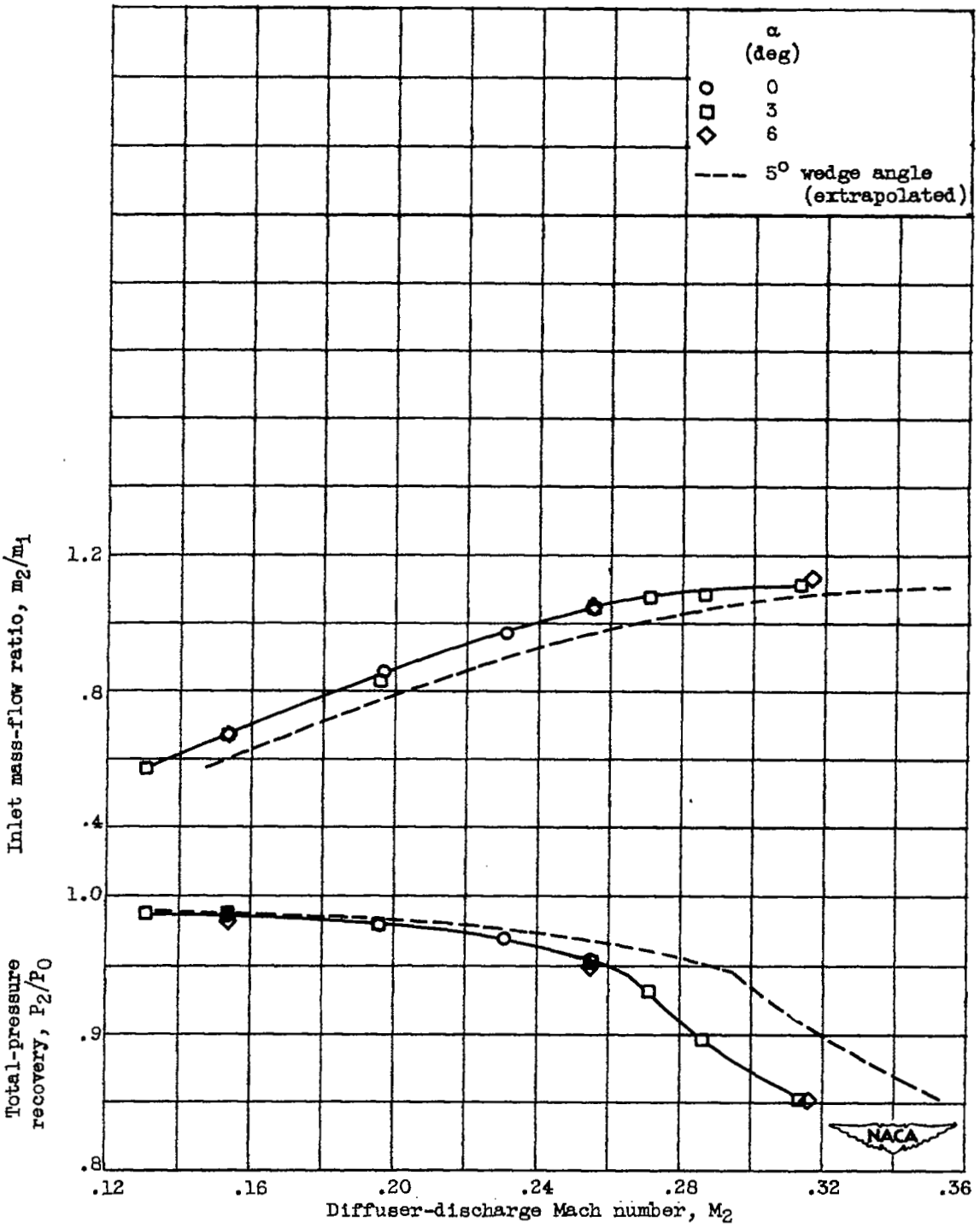

Figure 19. - Mass-flow and total-pressure recovery characteristics of 8°-wedge inlet utilizing boundary-layer scoop with sides for range of angles of attack from 0° to 6° at Mach number of 0.63.

[redacted]

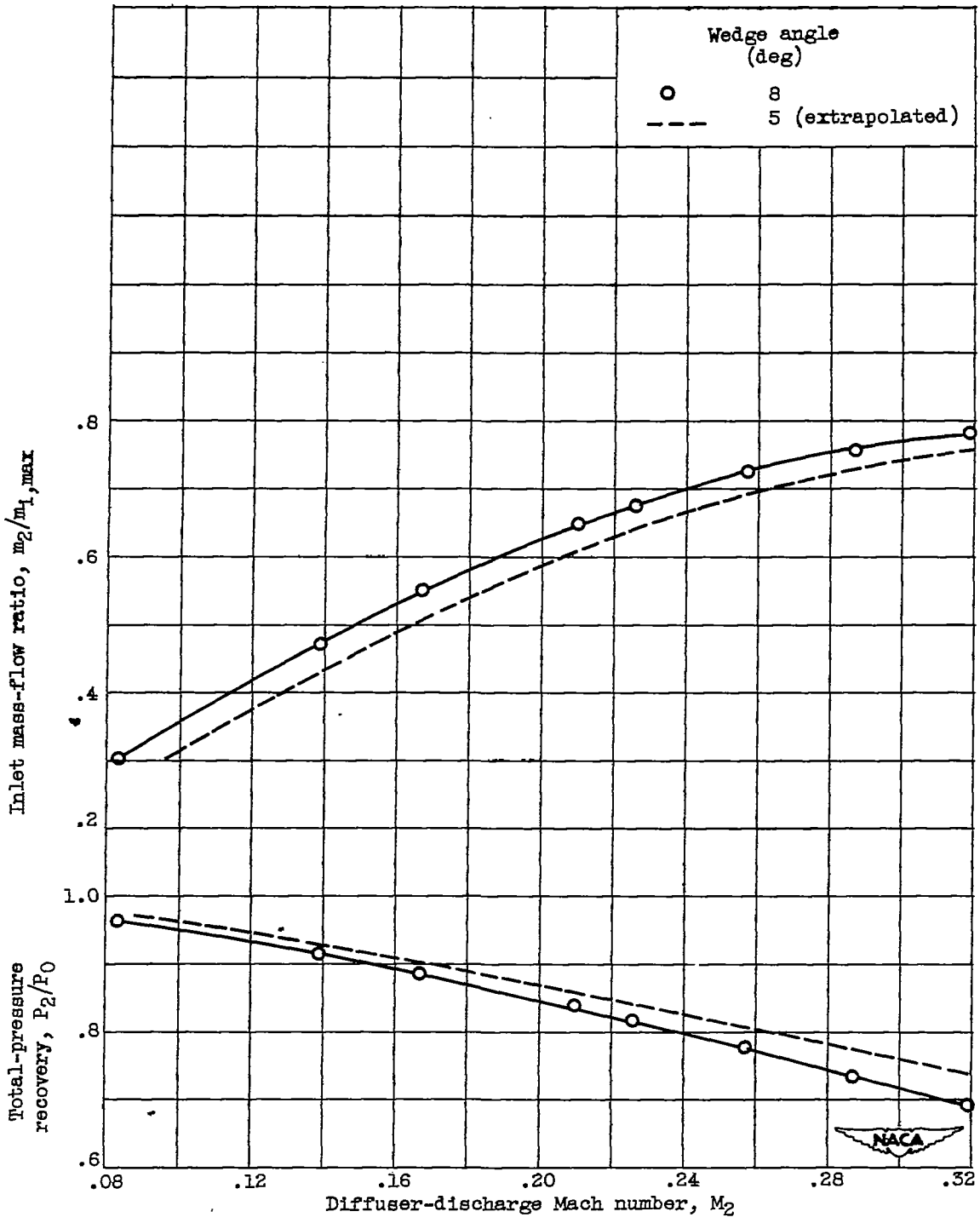

Figure 20. - Mass-flow and total-pressure recovery characteristics of 8°-wedge inlet at static take-off conditions (M_0, 0).

[redacted]

[redacted]